UNCLASSIFIED

AD NUMBER: AD0455160
LIMITATION CHANGES
TO: Approved for public release; distribution is unlimited.
FROM: Distribution authorized to US Government Agencies and their Contractors; Administrative/Operational Use; 1 Sep 1964. Other requests shall be referred to Office of Naval Research, Arlington, VA 22203.
AUTHORITY
ONR ltr dtd 23 Nov 1966

THIS PAGE IS UNCLASSIFIED

UNCLASSIFIED

AD 455160

DEFENSE DOCUMENTATION CENTER

FOR

SCIENTIFIC AND TECHNICAL INFORMATION

CAMERON STATION ALEXANDRIA, VIRGINIA

UNCLASSIFIED

NOTICE: When government or other drawings, specifications or other data are used for any purpose other than in connection with a definitely related government procurement operation, the U. S. Government thereby incurs no responsibility, nor any obligation whatsoever; and the fact that the Government may have formulated, furnished, or in any way supplied the said drawings, specifications, or other data is not to be regarded by implication or otherwise as in any manner licensing the holder or any other person or corporation, or conveying any rights or permission to manufacture, use or sell any patented invention that may in any way be related thereto.

CATALOGED BY DDC
AS AD No. 455160

SU-SEL-64-097

Low-Temperature Properties of Gallium Arsenide Diodes

455160

by

David J. Dumin

September 1964

Technical Report No. 5107-1

Prepared under
Office of Naval Research Contract
Nonr-225(24), NR 373 360
Jointly supported by the
U.S. Army Signal Corps, the
U.S. Air Force, and the U.S. Navy
(Office of Naval Research)

DDC
RECEIVED
JAN 28 1965
DDC-IRA C

SOLID-STATE ELECTRONICS LABORATORY

STANFORD ELECTRONICS LABORATORIES

STANFORD UNIVERSITY · STANFORD, CALIFORNIA

DDC AVAILABILITY NOTICE

Qualified requesters may obtain copies of this report from DDC. Foreign announcement and dissemination of this report by DDC is limited.

SEL-64-097

LOW-TEMPERATURE PROPERTIES OF GALLIUM ARSENIDE DIODES

by

David J. Dumin

September 1964

Reproduction in whole or in part
is permitted for any purpose of
the United States Government.

Technical Report No. 5107-1

Prepared under
Office of Naval Research Contract
Nonr-225(24), NR 373 360
Jointly supported by the U.S. Army Signal Corps,
the U.S. Air Force, and the U.S. Navy
(Office of Naval Research)

Solid-State Electronics Laboratory
Stanford Electronics Laboratories
Stanford University Stanford, California

ABSTRACT

The forward and reverse current-voltage characteristics of zinc-diffused gallium arsenide (GaAs) diodes have been investigated at temperatures between 300 and 4.2 °K. This study was initiated to explain the portions of the forward and reverse currents that are nonthermal in origin. The high-temperature current follows a law of the form $I = I_o \exp(qv/2kT)$. The low-temperature current follows a law of the form $I = I_1 \exp(\alpha v)$, where α is almost independent of temperature. The reverse current is higher at all temperatures and voltages than thermal-generation models predict and does not have the functional dependence associated with thermally generated currents.

Zinc-diffused GaAs diodes were produced and tested at temperatures between 300 and 4.2 °K. The doping densities of the parent materials ranged from $5 \cdot 10^{15}$ cm^{-3} to 10^{19} cm^{-3}. In addition to undoped n-type material, parent materials doped with selenium, sulfur, and tellurium were used. The p-type diffusions produced doping densities generally in the vicinity of 10^{20} cm^{-3}.

The high-temperature forward current has been explained in terms of existing thermal models using minority-carrier lifetimes of the order of 10^{-9} to 10^{-10} sec, and minority-carrier diffusion lengths of the order of 5μ. The low-temperature forward current has been explained in terms of a band-to-trap-to-band excess tunnelling model describable by two parameters: the effective tunnelling mass and the recombination probability. The effective tunnelling mass describes the exponent in the low-temperature current and the recombination probability describes the magnitude of the current. The effective masses observed in the forward direction scatter above and below the reduced hole-electron mass of $0.063\ m_o$. The temperature at which the tunnelling current dominates the forward characteristic rises as the doping density rises. The temperature at which the tunnelling current becomes appreciable has been described in terms of an "effective low temperature."

The reverse current has been explained in terms of a band-to-band tunnelling model at all temperatures below 300 °K. The effective tunnelling mass has been used as the parameter that describes the reverse current

and is observed generally to follow the effective masses found from the forward conduction. The experimentally measured reverse currents compare well with the theoretically predicted values.

The dominance of excess currents at low temperatures has been demonstrated in silicon in which two criteria are met: first, the carriers must remain mobile at low temperatures and, second, the space-charge region must be less than 1000 Å.

CONTENTS

Page

I. INTRODUCTION 1

II. THEORETICAL CONSIDERATIONS 3

A. General Tunnelling Model 3

1. Forward Tunnelling 7
2. Reverse Tunnelling 13

B. Effects of States in the Forbidden Band 15

C. Capacitance Information 16

III. EXPERIMENTAL CONSIDERATIONS 19

A. Sample Preparation 19

B. Experimental Techniques 20

C. Experimental Data 24

D. Bulk-Surface Current Determinations 26

IV. ANALYSIS OF DATA 31

A. Capacitance Studies 31

B. Forward Characteristics 36

C. Reverse Characteristics 45

D. Low-Bias Characteristics 50

E. High-Temperature Effects 52

F. Other Materials 55

G. Separation of Currents into Different Components 57

V. RESULTS AND DISCUSSION 61

VI. CONCLUSIONS 65

REFERENCES 67

TABLES

Number		Page
1	Diode description	20
2	Built-in voltages at 4.2 °K and 300 °K	33
3	Width constants at 4.2 °K and 300 °K	35
4	Degree of compensation in the junction region	37
5	Effective tunnelling masses at T = 4.2 °K and 300 °K as determined from the forward I-V characteristics	41
6	Effective tunnelling mass as determined from reverse I-V characteristics at 4.2 °K and 300 °K	48
7	High-temperature diode lifetime and diffusion length	55
8	Saturation currents of diode D10 at temperatures between 4.2 and 300 °K	58

ILLUSTRATIONS

Figure		Page
1	Schematic model of a p-n junction as an energy barrier	4
2	Model leading to excess current via deep traps in a forward-biased p-n junction	7
3	Average electron velocity in GaAs vs temperature for various electron concentrations	11
4	Reverse-tunnelling model	14
5	Rectangular barrier with and without traps	16
6	Linear model of a degenerate-p, degenerate-n junction	18
7	Schematic sketch of the sample holder	21
8	Thermometer calibration at $I_{diode} = 10^{-6}$ amp	22
9	Photograph of a typical diode showing method of measuring area	22
10	Schematic of I-V test circuit	23
11	Plots of forward I-V data on four samples of various doping densities	25
12	Forward I-V data on all samples	27
13	Reverse I-V data on all samples	28
14	Capacitance vs voltage for diode D160	28
15	Forward and reverse I-V characteristics at 300 °K and 4.2 °K for successively smaller areas of diode D300	29

Figure		Page

16 Area-perimeter comparison of currents 30

17 Built-in voltage as determined from capacitance data 32

18 Built-in voltage vs temperature 32

19 Junction width at 4.2 °K vs applied voltage for diode D160 . 34

20 Capacitance per unit area vs doping density for a step junction 35

21 Plot of N_D vs temperature for diode D160 37

22 Slope of log I-V characteristic vs doping density 38

23 Plots of log J vs $(V_{bi} - V_a)^{1/2}$ A/C 40

24 Effective tunnelling mass for various doping densities of the parent as determined from forward I-V characteristics 42

25 Temperature dependence of effective tunnelling mass as obtained from forward characteristics 42

26 Recombination probability as a function of applied bias . . 44

27 Recombination probability vs temperature for diode D160 at $V_a = 0.6$ v 45

28 Plots of log $J/[V_a \, C/A \, (V_g + V_a)]$ vs $(C/A \, (V_g + V_a)]^{-1}$. 46

29 Effective tunnelling mass for various doping densities of the parent as determined from reverse I-V characteristics 49

30 Temperature dependence of effective tunnelling mass as obtained from reverse characteristics 49

31 Plot of log $J/[V_a(V_a + V_g)^{1/2}]$ vs $(V_a + V_g)^{-1/2}$ for heavily doped samples 50

32 Reverse tunnelling current vs applied voltage at T = 4.2 °K 51

33 Low-level tunnelling currents at 300 °K and 4.2 °K 52

34 Log I - log V for low-voltage tunnelling current 53

35 Forward I-V characteristic of silicon diode HPA-69 57

36 Reverse data of Lowen and Rediker as analyzed by applying reverse tunnelling model at T = 300 °K 58

37 Forward current for temperatures between 300 °K and 4.2 °K . 59

38 Experimental data as the sum of three components of current 60

39 Effective low temperature for step junctions as a function of doping density 63

SYMBOLS

a	grading constant for a graded junction
A	diode area
A_I	incident particle flux
A_o	output particle flux
C	junction capacitance
$D(\mathcal{E})$	energy distribution function
E	electrical field
E_{av}	average electric field
E_{max}	maximum electric field
$\mathcal{E}$	energy
$\mathcal{E}_b$	energy barrier in electron volts
$\mathcal{E}_C$	conduction band edge
$\mathcal{E}_F$	Fermi energy
$\mathcal{E}_F(0)$	Fermi energy at $T = 0$ °K
$\mathcal{E}_G$	energy gap in electron volts
$\mathcal{E}_V$	valence band edge
$h, \hbar$	Planck's constant, Planck's constant/2π
i	$\sqrt{-1}$
I	current
I_o	saturation current
$I_o(\mathrm{dif})$	diffusion current at $V_a = 0$ v
$I_o(\mathrm{rec})$	recombination current at $V_a = 0$ v
$I_o(\mathrm{tun})$	tunnelling current at $V_a = 0$ v
J	current density

J_I	incident current density
J_T	tunnelling current density
k	Boltzmann's constant
L_o	minority-carrier diffusion length
m	mass
m_o	electron rest mass
m_e	conductivity mass of an electron
m_h	conductivity mass of a hole
m_T	effective tunnelling mass
n	electron concentration
n_i	intrinsic carrier concentration
n_I	number of particles incident upon a barrier
N	particle concentration
N_A	acceptor concentration
N_D	donor concentration
p	hole concentration
p(x)	classical momentum
P_R	recombination probability
P_T	tunnelling probability
q	electronic charge
T	absolute temperature
T_{eff}	effective low temperature
$u, u(\mathcal{E})$	particle velocity
u_I	velocity of incident particles
$\bar{u}$	average particle velocity
v, V	voltage

V_b	energy barrier in volts
V_g	energy gap in volts
V_a	applied voltage
V_{bi}	built-in voltage
V_{g0}	energy gap in volts at $T = 0\ ^\circ K$
w	width of the space-charge region
W_1	width constant; width of space-charge region at 1 v total bias
x	position coordinate
α	exponent of low-temperature I-V characteristic
γ	temperature coefficient of recombination probability
ϵ	dielectric constant
ϕ_n, ϕ_p	Fermi level of electrons or holes
τ	minority-carrier lifetime
$\phi(x)$	amplitude factor in wave function
$\psi(x)$	wave function

ACKNOWLEDGMENT

The author would like to thank the various members of the Solid State Laboratory at Stanford for their many helpful suggestions during the course of this investigation. In particular, I would like to thank Prof. G. L. Pearson for his guidance and encouragement during the performance of this work, and Prof. J. L. Moll for the many stimulating discussions of the theoretical aspects of this work. I would also like to thank Prof. J. F. Gibbons, who originally suggested the topic of this research.

I. INTRODUCTION

The properties of semiconductor diodes have been well analyzed in terms of diode parameters and temperature. Forward and reverse characteristics dominated by diffusion of minority carriers in nondegenerate materials have been treated by Shockley [Ref. 1]. In relatively wide band-gap materials such as silicon the characteristics have been analyzed by Sah, Noyce, and Shockley in terms of generation and recombination via deep traps [Ref. 2]. These two theories are based upon thermal excitation of carriers. As the temperature is lowered the carriers become bound on donor or acceptor sites. A phenomenon known as double injection has been discussed by Lampert [Ref. 3] in semiconductors and insulators in which carriers have been excited out of bound states. Double injection is also observed in p-n junctions in which one side of the junction or the space-charge region becomes insulating at low temperatures [Ref. 4]. The extension of diode characteristics to degenerate materials was appreciably advanced with the observation of tunnelling and the analysis of tunnel (Esaki) diodes by Esaki, and Esaki and Miyahara [Ref. 5]. The appearance of excess current in tunnel diodes was reported by these authors. This current is the current that flows at forward biases greater than that associated with tunnelling but less than that associated with normal diode currents. This excess current has been shown to be related to tunnelling via deep traps by Chynoweth, Feldmann, and Logan in their work on irradiated silicon and germanium tunnel diodes [Ref. 6]. The discussion of the reverse characteristics of narrow silicon and germanium p-n junctions was presented by Chynoweth, et al [Ref. 7] in terms of a tunnelling model.

The present study was undertaken in an attempt to explain the characteristics of GaAs-diffused diodes at temperatures between 300 °K and 4.2 °K in terms of the thermal model at high temperatures and the tunnelling model at low temperatures. The bulk of the effort has been concentrated on the low-temperature tunnelling model.

The investigation into the low-temperature properties of GaAs diodes was prompted by the announcement of a low-temperature thermometer by Cohen, Snow, and Tretola [Ref. 8]. This thermometer was a forward-biased

GaAs diode. With a constant current of 10^{-6} amp through the diode, the voltage across the diode increased from 0.7 v at 300 °K, to 1.4 v at 4.2 °K. Examination of the I-V characteristic of this diode thermometer showed the diode to have a forward current of the form $I = I_o \exp(qv/2kT)$ for temperatures above 100 °K. Below 100 °K the diode forward current followed $I = I_1 \exp(\alpha v)$, where α is almost independent of temperature. A similar temperature-independent exponent was observed in silicon tunnel diodes in the excess current region by Chynoweth, Feldmann, and Logan at 300 °K and 4.2 °K [Ref. 6]. It was decided to apply an excess tunnelling current model to the GaAs diodes. A similar tunnelling model had been suggested by Nelson, et al [Ref. 9] and by Archer, et al [Ref. 10] to explain the high-level injection properties of GaAs luminescent junctions. If the low-temperature current is excess tunnel diode current, then the current-voltage characteristic should be sensitive to the width of the space-charge region. A series of step and graded junctions with various widths for the space-charge region were produced and the diode characteristics of these junctions were compared with an excess tunnel current model in the forward direction. These diodes were produced by diffusion of zinc into n-type GaAs of varying doping density. The applicability of the excess-current approach to the forward characteristic has led to an application of band-to-band tunnelling to the reverse characteristic. The reverse characteristics of the diodes were tested from 300 to 4.2 °K and compared to existing models of tunnel diodes.

II. THEORETICAL CONSIDERATIONS

A. GENERAL TUNNELLING MODEL

If an electron is incident upon a potential barrier, there is a quantum-mechanical tunnelling probability associated with penetration of the electron into or through the barrier. Various techniques are available for the calculation of this tunnelling probability. If the potential varies smoothly across the barrier, a simple and fairly accurate technique is to use an approximation developed by Wentzel, Kramers, and Brillouin [Ref. 11], usually referred to as the WKB approximation. Under this approximation the wave function is written as

$$\psi(x) = \phi(x) \exp\left(\pm \frac{i}{\hbar} \int_0^x p(x)\, dx\right) \tag{1}$$

where $\psi(x)$ is the wave function of the electron, $\phi(x)$ is a slowly varying function of position, $i = \sqrt{-1}$, $\hbar$ is Planck's constant/2π, and $p(x)$ is the classical momentum given by $\sqrt{2m\mathcal{E}}$. Here the integral extends over the region of interest, $\mathcal{E}$ is the energy of the electron, and m is its mass. This approximation is valid if $\hbar$ is small compared to the action. In practical terms the WKB approximation is valid if the mass is large, the energy high, and the potential smooth.

The WKB approximation can be applied to the situation that exists within a p-n junction [Ref. 12]. A schematic sketch of a p-n junction is shown in Fig. 1. Here a particle of charge q and mass m is incident upon a barrier of height $\mathcal{E}_b$ containing a field $E(x)$. The propagation constant is imaginary to the right and left of the barrier and real within the barrier. These propagation constants correspond to travelling waves in the p and n regions and a wave that decays exponentially in the space-charge region.

An approximation must be made for the mass of the tunnelling particle. Consider the case of band-to-band tunnelling from the p-side to the n-side. A hole is incident from the left upon the barrier. On the p-side of the barrier the hole can be assumed to have a mass m_h, which is the conduction

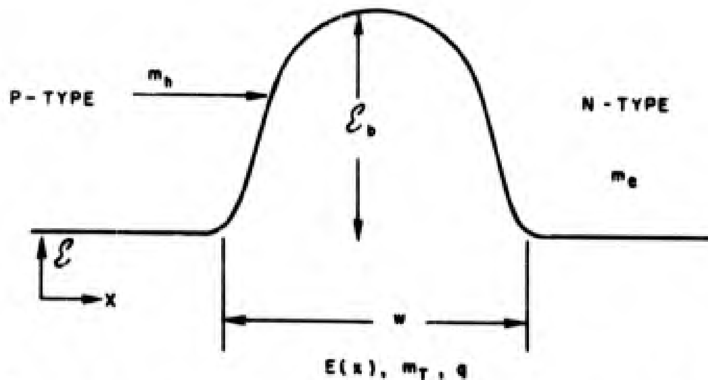

32037 FIG. 1. SCHEMATIC MODEL OF A p-n JUNCTION AS AN ENERGY BARRIER.

mass of holes in the valence band. On the n-side of the barrier the particle must have the electron conduction mass m_e. This leads to an approximation for the mass of the tunnelling particle. The reduced hole-electron mass,

$$m_T = \frac{m_e m_h}{m_e + m_h} \tag{2a}$$

is often used as the mass of the tunnelling particle. If the recombination of the holes and electrons is assumed to take place at the position in the junction where the hole and electron populations are equal, then the tunnelling mass would be

$$m_T = \frac{m_e m_h}{m_e + m_h + 2\sqrt{m_e m_h}} \tag{2b}$$

Thus, using the values of conduction mass of holes and electrons in lightly doped GaAs, $m_e = 0.072\ m_o$ and $m_h = 0.5\ m_o$ [Ref. 13], the two tunnelling masses are:

$$m_T(\text{Eq. 2a}) = 0.063\ m_o$$

and

$$m_T(\text{Eq. 2b}) = 0.050\ m_o$$

where m_o is the electron rest mass. These tunnelling masses have been calculated on the basis of hole and electron conduction masses given for lightly doped GaAs. The tunnelling mass will be expected to vary somewhat with temperature and doping density since the conduction masses will tend to vary somewhat. Under large forward bias where band-to-trap-to-band tunnelling is considered, the end state of the tunnelling process will probably also affect the tunnelling mass. The effective mass approximation applied to a p-n junction involves using one of the reduced masses given in Eqs. (2a) or (2b) for the mass of the tunnelling particle.

Under the WKB approximation the transmission coefficient or the tunnelling probability is given by

$$P_T = \exp - \left(\frac{1}{\hbar} \int_0^x \sqrt{2m\mathcal{E}}\ dx \right) \tag{3}$$

where P_T is the tunnelling probability. Application of this integral to the tunnelling model of Fig. 1 results in a tunnelling probability of [Ref. 12]

$$P_T = \exp - \left(\frac{\pi m_T^{1/2}\ \mathcal{E}_b^{3/2}}{2\sqrt{2}\ qhE} \right) \tag{4}$$

where m_T is the effective tunnelling mass defined in Eqs. (2a) or (2b), $\mathcal{E}_b$ is the energy barrier through which the particle must tunnel, in electron volts, and E is the electric field within the barrier.

In materials such as germanium and silicon in which indirect transitions must be considered, the tunnelling probability must be considerably modified to account for the conservation of perpendicular momentum. In GaAs the transitions are considered to be direct.

A fairly basic assumption involving the field within a p-n junction is involved in the calculation of Eq. (4). The field within a junction varies with distance and the more accurate estimates of $E(x)$ cannot be integrated under the WKB approximation to yield Eq. (4). Thus the linear field is used to derive Eq. (4). The value of the field that must appear in Eq. (4) thus lies between the average and the maximum field values, $E_{av} < E < E_{max}$. The average field is given by

$$E_{av} = \frac{V_g + V_a}{w} \tag{5a}$$

where V_g is the band gap, V_a is the applied voltage, and w is the junction width. The maximum field is given by

$$E_{max} = \frac{2(V_g + V_a)}{w} \tag{5b}$$

for a step junction, and

$$E_{max} = \frac{3/2\ (V_g + V_a)}{w} \tag{5c}$$

for a graded junction. The maximum field is used throughout this study for the constant field within the junction. The use of the maximum field for the value of the field within the junction is the basis of the constant field approximation.

The tunnelling current can now be calculated by considering the number of particles incident upon a barrier and multiplying this quantity by the tunnelling probability. The tunnelling probability is then modified by the probability that the initial state is occupied and the end

state is vacant. Tunnelling currents are calculated for both forward- and reverse-biased p-n junctions in the following two subsections. The general form for the current is

$$J = q \times n_I \times u_I \times P_T \times P_R \tag{6}$$

where n_I is the incident particle density, u_I is the incident particle velocity, and P_R is the recombination probability, which here is used to account for the condition of the end state. The recombination probability is used to account for the existence of states in the band gap leading to excess current in the forward direction. It does not appear in the reverse tunnelling calculations; and under reverse bias, $P_R \equiv 1$.

1. Forward Tunnelling

In this section the general tunnelling model is specialized to account for tunnelling in the forward direction. The tunnelling is discussed in terms of the model described in Fig. 2. The tunnelling process consists of a particle incident upon the potential barrier at point (a), tunnelling to a state at point (b), and from there recombining with a hole

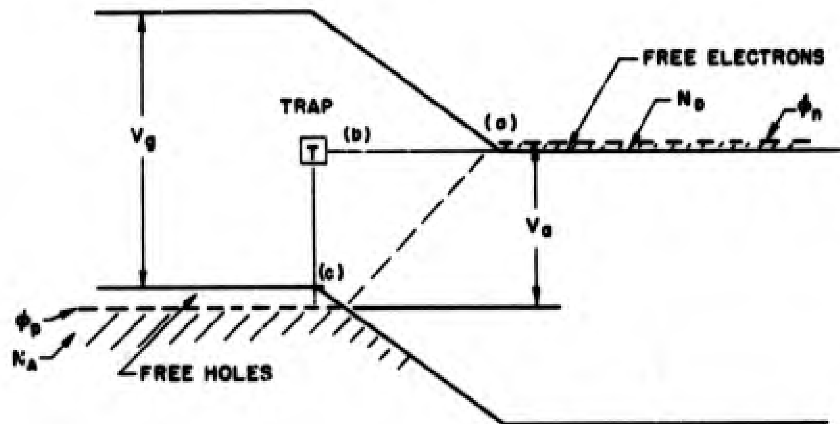

32038

FIG. 2. MODEL LEADING TO EXCESS CURRENT VIA DEEP TRAPS IN A FORWARD-BIASED p-n JUNCTION.

in the valence band at point (c). This model is quite similar to existing models for excess current in normal tunnel diodes [Ref. 6]. The incident particle velocity is first calculated. This velocity multiplied by the particle density and electron charge is the incident current. The tunnelling current is the incident current multipled by the tunnelling probability and recombination probability. The tunnelling probability is written in terms of junction parameters to represent certain features of the current-voltage characteristic.

The incident current at point (a) can be calculated by multiplying the particle density in the conduction band by an average velocity. The average velocity $\bar{u}$ can be found by averaging of the velocity distribution $u(\mathcal{E})$ over the energy distribution $D(\mathcal{E})$, and normalizing the result to yield,

$$\bar{u} = \frac{\int_0^\infty D(\mathcal{E})\, u(\mathcal{E})\, d\mathcal{E}}{\int_0^\infty D(\mathcal{E})\, d\mathcal{E}} \tag{7}$$

Here the integral extends over the full energy distribution. At low temperatures such that the thermal spread in the carrier distribution is small compared to the position of the Fermi level, the integration can be carried out between $0 < \mathcal{E} < \mathcal{E}_F$, where $\mathcal{E}_F$ is the Fermi level or Φ_n in Fig. 2. Under this approximation, the Fermi level becomes discontinuous and [Ref. 14, p. 384]

$$\mathcal{E}_F(T) = \mathcal{E}_F(0)\left[1 - \frac{\pi^2}{12}\left(\frac{kT}{\mathcal{E}_F(0)}\right)^2 - \frac{\pi^4}{80}\left(\frac{kT}{\mathcal{E}_F(0)}\right)^4 + \dots\right] \approx \mathcal{E}_F(0) \tag{8}$$

if $\mathcal{E}_F(0) << kT$. Here k is Boltzmann's constant and T is the absolute temperature. Thus, using

$$D(\mathcal{E}) \propto \mathcal{E}^{1/2}$$

and

$$u(\mathcal{E}) = \left(\frac{2\mathcal{E}}{m_e}\right)^{1/2} \tag{9}$$

Eq. (7) can be integrated directly to yield

$$\bar{u} = \frac{\int_0^{\mathcal{E}_F(0)} \mathcal{E}^{1/2} \left(\frac{2\mathcal{E}}{m_e}\right)^{1/2} d\mathcal{E}}{\int_0^{\mathcal{E}_F(0)} \mathcal{E}^{1/2} \, d\mathcal{E}} = \sqrt{\frac{9\mathcal{E}_F(0)}{8m_e}} \tag{10}$$

The value of $\mathcal{E}_F(0)$ can be related to the particle density N in a Fermi gas by [Ref. 15, p. 301]

$$\mathcal{E}_F(0) = \frac{h^2}{2m_e} \left(\frac{3}{8\pi}\right)^{2/3} N^{2/3} \tag{11}$$

When finding the particle velocity in a given direction, a factor of $\sqrt{1/6\pi}$ arises in Eq. (10) to account for the integration over the spatial angles. The low-temperature approximation that is made in this paper is essentially given in Eq. (8), where the Fermi level is considered to be discontinuous. Assuming the Fermi level to be discontinuous avoids complicated density-of-states functions near the Fermi level.

The effect of temperature can now be included in the average velocity in a rough manner. In a Maxwellian gas the temperature and the thermal velocity are related by

$$\bar{u}_{th} = \left(\frac{3kT}{m_e}\right)^{1/2} \tag{12}$$

Use of Eq. (11) in Eq. (10) to govern the low-temperature range of velocities, and Eq. (12) to govern the high-temperature range, leads to the results presented in Fig. 3. Here the velocity of the particles is approximated by the sum of the Fermi velocity and the Maxwellian velocity and is plotted for various values of the electron density n.

The electron current incident on the barrier from the n-type material can be written as

$$J_I = (\sqrt{1/6\pi})(q\ n\ \bar{u}) = (\sqrt{1/6\pi})(q\ N_D\ \bar{u}) \qquad (13)$$

assuming that all of the donors, N_D, are ionized and contribute to the density of conduction electrons. The electron velocity $\bar{u}$ is found from the curves of Fig. 3 once the doping density and temperature are known.

The tunnelling current J_T can be written as

$$J_T = J_I\ P_T\ P_R \qquad (14)$$

States in the forbidden gap will lead to structure in the excess current of tunnel diodes [Ref. 16] and to a general increase in the excess current due to alterations in the barrier through which the electron must tunnel [Ref. 17]. In many materials these states have been associated with impurities [Ref. 16] or with phonons [Ref. 18]. It should be noted that in the absence of direct tunnelling from the conduction to the valence band these states are responsible for the excess current that flows under this model.

The tunnelling probability can be expressed in terms of the diode parameters by expressing the energy barrier $\mathcal{E}_b$ and the electric field E_{max} in terms of the junction parameters. Under application of forward bias V_a,

$$E_{max} = \frac{2(V_{bi} - V_a)}{w} \qquad (15)$$

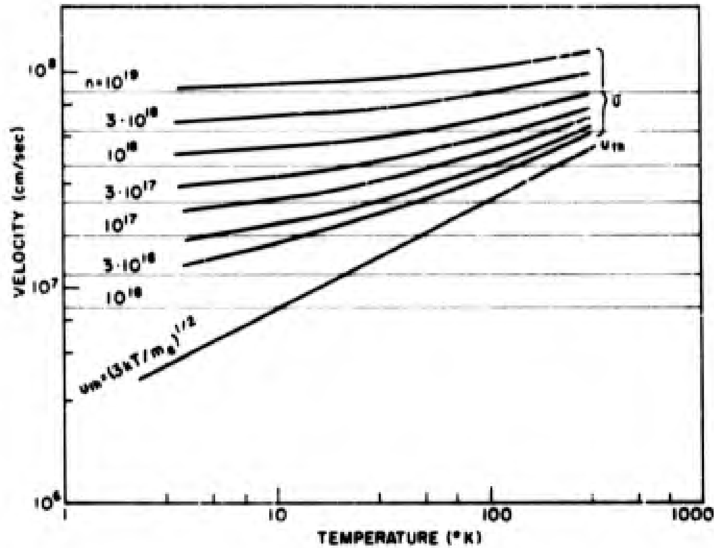

32039

FIG. 3. AVERAGE ELECTRON VELOCITY IN GaAs VS TEMPERATURE FOR VARIOUS ELECTRON CONCENTRATIONS.

and

$$\mathcal{E}_b = q(V_{bi} - V_a) \tag{16}$$

where V_{bi} is the built-in voltage. There is some doubt as to what value of built-in voltage should be used in Eqs. (15) and (16). The values chosen usually range from $V_g + 0.6(\phi_n + \phi_p)$ to $V_g + \phi_n + \phi_p$ [Refs. 6 and 19] where the symbols have the meaning shown in Fig. 2. Both of these values predict built-in voltages which are in excess of the energy gap. The built-in voltages measured for diodes with one or both sides of the junction degenerate are less than these values and in fact are less than the band gap. The values of V_{bi} determined from capacitance measurements will be used in Eq. (15) and Eq. (16) rather than either of the values that predict voltages larger than the band gap. There is some justification for this approach since the space-charge region does not start until the Fermi levels cross the conduction or valence band. This type of consideration leads to a built-in voltage slightly less than the band gap for degenerate materials.

The width w of the space-charge region can be written in terms of the diode area A and the measured diode low-frequency capacitance C as

$$w = \epsilon A/C \tag{17}$$

where ϵ is the dielectric constant. The tunnelling probability can be written as

$$P_T = \exp - \left[\frac{\pi q^{1/2} m_T^{1/2} (V_{bi} - V_a)^{1/2} A\epsilon}{4\sqrt{2}\, \hbar\, c} \right] \tag{18}$$

and the tunnelling current as

$$J_T = \frac{q N_D \bar{u} P_R}{\sqrt{6\pi}} \exp - \left[\frac{\pi q^{1/2} m_T^{1/2} (V_{bi} - V_a)^{1/2} A\epsilon}{4\sqrt{2}\, \hbar\, c} \right] \tag{19}$$

The tunnelling current assumes a simple form under the assumption that the density of states in the band gap is relatively independent of energy. For a nondegenerate step junction

$$\frac{C}{A} = \sqrt{\frac{q\, \epsilon\, N_D N_A}{2(V_{bi} - V_a)(N_D + N_A)}} \approx \sqrt{\frac{q\, \epsilon\, N_D}{2(V_{bi} - V_a)}} \tag{20}$$

where N_A is the acceptor concentration. The tunnelling current becomes

$$J_T = \frac{q N_D \bar{u} P_R}{\sqrt{6\pi}} \exp - \left[\frac{\pi m_T^{1/2} (V_{bi} - V_a)\, \epsilon^{1/2}}{4\, \hbar\, N_D^{1/2}} \right] \tag{21a}$$

or

$$J_T = B \exp\,[\alpha V_a] \tag{21b}$$

where

$$B = \frac{q\ N_D\ \bar{u}\ P_R}{\sqrt{6\pi}} \exp - \left[\frac{\pi\ m_T^{1/2}\ V_{bi}\ \epsilon^{1/2}}{4\ \hbar\ N_D^{1/2}}\right] \tag{22a}$$

and

$$\alpha = \frac{\pi\ m_T^{1/2}\ \epsilon^{1/2}}{4\ \hbar\ N_D^{1/2}} \tag{22b}$$

Thus in a step junction with uniform trap density in the band gap, the excess current should be an exponential function of applied voltage and should have the temperature dependences associated with N_D, $\bar{u}$, V_{bi}, and m_T. For a general junction, Eq. (19) gives a useful functional form to use in evaluating the diode characteristics.

2. Reverse Tunnelling

The theory of tunnelling in reverse-biased p-n junctions has been considered extensively [Ref. 7, Ref. 12]. The results of these considerations are presented here. As in the case of tunnelling in the forward direction, the low-temperature approximations are made. The model chosen is shown in Fig. 4 where all voltages and energies are defined.

The current that flows under reverse bias can be written as

$$J_T = J_I\ P_T$$

which is the product of the incident current times the tunnelling probability. The incident current can be calculated by first finding the particle density in k-space and then integrating this over the junction region. The result of this type of calculation is [Ref. 20, p. 253]

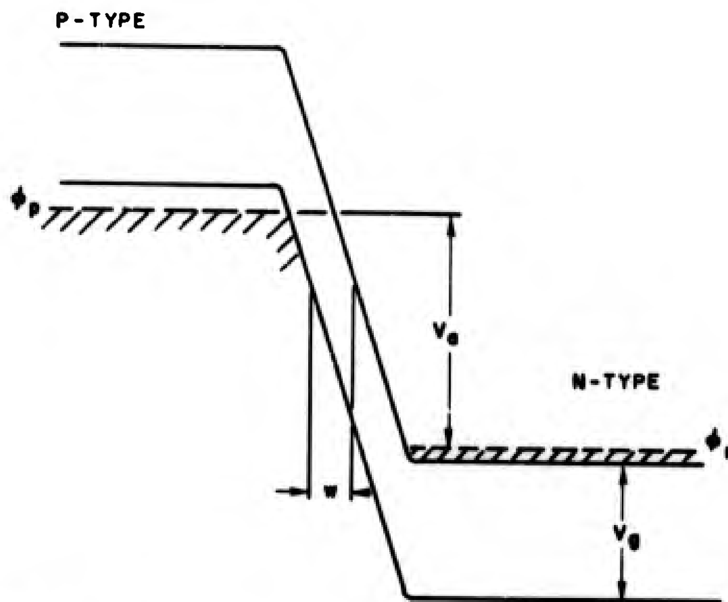

FIG. 4. REVERSE-TUNNELLING MODEL.

$$J_I = \frac{\sqrt{2}\, q^3\, m_T^{1/2}\, V_a\, E}{4\pi^3\, \hbar^2\, q^{1/2}\, V_g^{1/2}} \tag{23}$$

The tunnelling probability can be written as

$$P_T = \exp - \left[\frac{\pi\, m_T^{1/2}\, \mathcal{E}_b^{3/2}}{2\sqrt{2}\, q\, \hbar\, E} \right] \tag{24}$$

In the reverse-biased junction the energy barrier becomes the band gap. Under the constant field approximation the reverse-tunnelling current becomes

$$J_T = \frac{\sqrt{2}\, q^3\, m_T^{1/2}\, V_a (V_g + V_a) C}{2\pi^3\, \hbar^2\, q^{1/2}\, V_g^{1/2}\, \epsilon\, A} \exp - \left[\frac{\pi m_T^{1/2}\, q^{1/2}\, V_g^{3/2}\, \epsilon\, A}{4\sqrt{2}\, \hbar\, (V_g + V_a) C} \right] \tag{25}$$

As in the case of forward tunnelling, this form for the reverse current can be adapted to step or graded junctions. The relative simplicity of Eq. (25) does not usually varrant specializing Eq. (25) to a specific type of junction.

The temperature dependence of the reverse-tunnelling mass can be determined from the measured values of the temperature dependence of capacitance and the temperature dependence of the band gap. For high doping densities where Φ_p is much greater than kT/q, the effects of temperature will be small. At $p = 10^{20}\ cm^{-3}$, $\Phi_p = 0.160$ v. Thus it is considered justified to neglect temperature for $T \leq 300\ ^{\circ}K$.

B. EFFECTS OF STATES IN THE FORBIDDEN BAND

The effects of states in the forbidden band, or the effects of deep traps, can influence both the forward and reverse characteristics. Of the effects that have been treated [Refs. 6, 17, and 19], only the simplest are considered here.

In the forward direction deep traps will produce two dominant effects. The first will be an increase in the current whenever the electron distribution finds itself adjacent to a high density of traps. This band-to-trap-to-band tunnelling is in many ways similar to the band-to-band tunnelling observed in Esaki diodes, except that here the high density of available states is provided by a deep trap level rather than the unfilled valence band. Sufficient doping with deep traps can provide negative resistance regions in the excess current portion of the I-V characteristic.

The second effect that can appear is a general increase in the excess current with increased density of deep traps. The effect of the deep trap is to provide a region in which the electron can classically oscillate. This region in effect lowers the tunnelling distance. The model associated with tunnelling through a deep trap is shown in Fig. 5.

Deep traps increase the reverse-tunnelling current. The effect is similar to that causing a general increase in the forward current. Both of the increases suggested in the forward and reverse direction assume that the rate-limiting process is associated with the tunnelling probability and not with the lifetime in the deep trap.

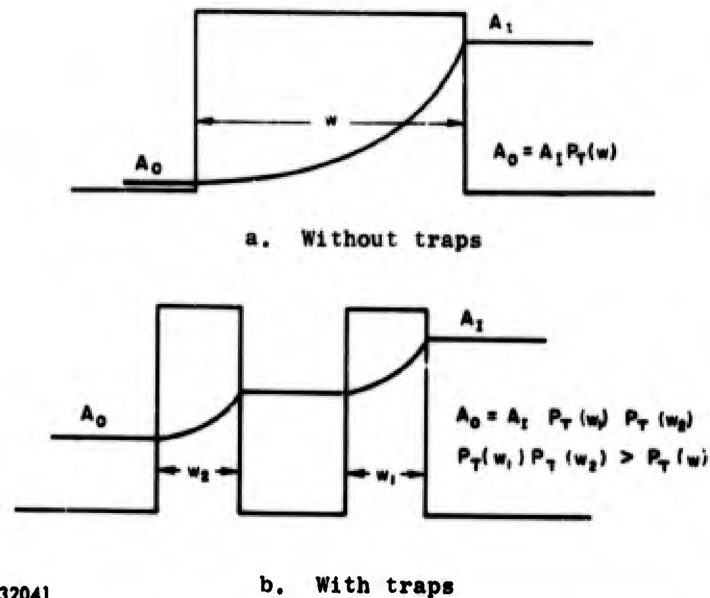

FIG. 5. RECTANGULAR BARRIER WITH AND WITHOUT TRAPS.

C. CAPACITANCE INFORMATION

The capacitance vs applied voltage can provide useful data concerning the junction parameters. In this section the information available from capacitance data will be discussed.

The capacitance of a nondegenerate step junction is given as [Ref. 21, p. 60]

$$C = A\sqrt{\frac{q\,\epsilon\,N_D\,N_A}{2(V_{bi} - V_a)(N_D + N_A)}} \tag{26a}$$

For a diode which is heavily doped on the p-side and much more lightly doped on the n-side, Eq. (26a) reduces to

$$C = A\sqrt{\frac{q\,\epsilon\,N_D}{2(V_{bi} - V_a)}} \tag{26b}$$

The capacitance of a linearly graded junction is given by [Ref. 21, p. 61]

$$C = A \left[\frac{a\, q\, \epsilon^2}{12(V_{bi} - V_a)} \right]^{1/3} \qquad (26c)$$

where a is the grading constant. The type of junction under study can be determined from a plot of C^{-2} or C^{-3} as a function of applied voltage. The intercept of this plot at $C^{-2} = 0$ or $C^{-3} = 0$ with the voltage axis is a measure of the built-in voltage.

The capacitance is an indication of whether or not the donors or acceptors are ionized. The capacitance as given in Eqs. (26) is only applicable as long as the carriers are ionized. If either the donors or acceptors freeze out at low temperatures, then the capacitance of the junction will go to zero and the voltage dependence of Eqs. (26) will not apply.

The formulas given above for junction capacitance are strictly valid only for junctions in which both sides are nondegenerate. The measured values of V_{bi} are usually somewhat less than the values calculated on the basis of Eqs. (26), particularly in a junction in which one or both sides are degenerate. In this case Eqs. (26) should be considered to be quite approximate.

If the nondegenerate approximations are made to the degenerate junction, then the built-in voltage can be calculated to be nearly $V_g + \phi_p + \phi_n$, where the symbols are defined in Fig. 6. That the built-in voltage is always less than the band gap can be seen by noting that when an applied voltage equal to the band-gap voltage is applied to the junction in Fig. 6, the depletion region no longer exists. The electron and hole distributions have essentially merged. The depletion region does not start until the Fermi level (or quasi Fermi level) drops below the conduction band edge for electrons or above the valence band edge for holes. If it is further assumed that the built-in voltage is a measure of this voltage difference minus any voltage difference associated with Debye lengths on either side of the junction, it is seen that the built-in voltage measured should be less than the band gap.

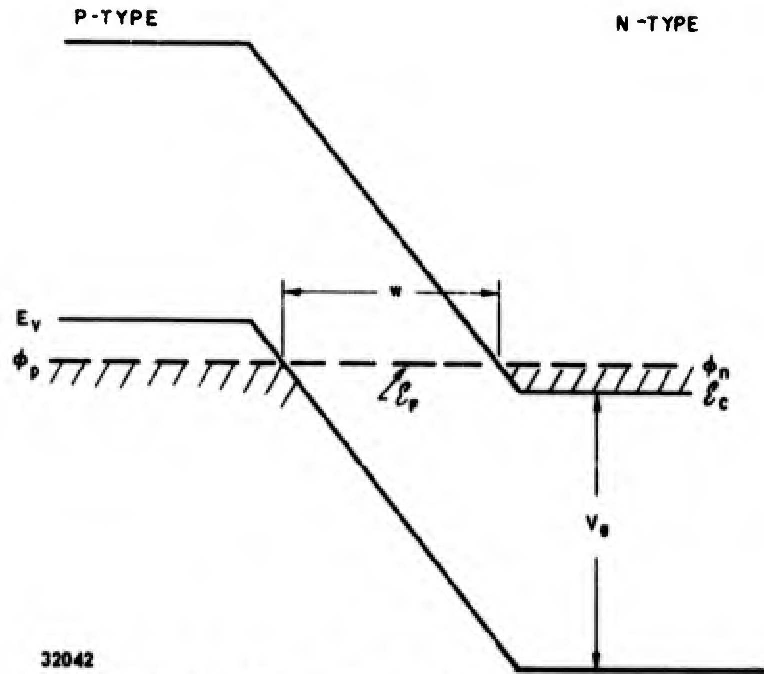

FIG. 6. LINEAR MODEL OF A DEGENERATE-p, DEGENERATE-n JUNCTION.

III. EXPERIMENTAL CONSIDERATIONS

A. SAMPLE PREPARATION

The samples described in this work were diodes produced by closed-tube diffusion of zinc or manganese into n-type GaAs. Elemental zinc was used when a high hole concentration ($p = 10^{20}$ cm^{-3}) was desired, and zinc-gallium alloys were used when lower hole concentrations were desired. The results of Casey [Ref. 22] were used to predict the approximate hole concentrations associated with various zinc-gallium alloys. All diffusions were performed at 900 °C.

The cleaning of the materials and diffusion of the zinc into the GaAs followed the procedure described in Ref. 22. The diffusion times varied depending on the depth of diffusion required and the source of diffusion. After diffusion the sample was removed from the ampoule and the surface zinc was removed by a half-hour etch in dilute HCl. The sample was lapped on one side to produce a structure about one-half of the original thickness, exposing n-type material. The sample was given a 3-sec etch in a solution of 90% HNO_3-10% HF and quenched in methanol. This clean-up etch left both p and n surfaces fairly shiny and smooth.

Ohmic contacts were provided to the n-side by evaporating and alloying a mixture of 50% gold - 50% tin at 450 °C. Ohmic contacts were provided to the p-side by evaporating and alloying 98% gold - 2% cadmium at 450 °C. The resulting chip was scribed and broken into convenient-sized pieces. Some of the smaller pieces were tested directly. Mesa diodes were formed on the larger chips. The current densities of the mesa diodes and the cleaved diodes were compared and were found to yield identical results.

The properties of the samples tested are described in Table 1. Some GaAs diodes provided by outside laboratories were also tested and are included in this table. A few silicon samples were tested. These diodes were provided by hp Associates* and were grown junctions with relatively narrow space-charge layers separating degenerate p and n regions.

*An affiliate of Hewlett-Packard Co., Palo Alto, Calif.

TABLE 1. DIODE DESCRIPTION

Diode Number	Donor Concentration and Dopant of Parent (cm^{-3})	Diffusion Source	Diffusion Time	Approximate Hole Concentration (cm^{-3})
D10	$3.1 \cdot 10^{17}$ (Te)	100% Zn	5 min	$2 \cdot 10^{20}$
D100	$3.1 \cdot 10^{17}$ (Te)	0.21% Zn in Ga	16 hr	$3.5 \cdot 10^{18}$
D130	$6.1 \cdot 10^{15}$ --	100% Zn	5 min	$2 \cdot 10^{20}$
D150	$2.5 \cdot 10^{16}$ --	100% Zn	5 min	$2 \cdot 10^{20}$
D160	$4.6 \cdot 10^{18}$ (Te)	100% Zn	5 min	$2 \cdot 10^{20}$
D180	$3.1 \cdot 10^{17}$ (Te)	100% Mn	4 hr	--
D260	$4.3 \cdot 10^{18}$ (S)	100% Zn	5 min	$2 \cdot 10^{20}$
D290	$8.3 \cdot 10^{18}$ (Te)	100% Zn	5 min	$2 \cdot 10^{20}$
D300	$2.1 \cdot 10^{18}$ (Se)	100% Zn	5 min	$2 \cdot 10^{20}$
D310	$9.4 \cdot 10^{18}$ (Se)	100% Zn	5 min	$2 \cdot 10^{20}$
D320	$1.8 \cdot 10^{18}$ (Te)	100% Zn	5 min	$2 \cdot 10^{20}$
D340	$5.0 \cdot 10^{17}$ (Te)	100% Zn	5 min	$2 \cdot 10^{20}$
D350	$1.0 \cdot 10^{17}$ (Te)	100% Zn	5 min	$2 \cdot 10^{20}$
D380	$4.6 \cdot 10^{18}$ (Te)	100% Zn	5 min	$2 \cdot 10^{20}$
HPA-1	$1.0 \cdot 10^{17}$ (Te)	--	--	--
EN-01	$2 \cdot 10^{17}$ --	4% Zn in Ga	16 hr at 850 °C	$2 \cdot 10^{19}$
HPA-69	p^+-n^+ silicon grown junction			

Te - tellurium
Se - selenium
Zn - zinc
Ga - gallium
Mn - manganese
S - sulfur

B. EXPERIMENTAL TECHNIQUES

After the diodes had been etched to form mesas or had been cleaved, they were mounted in the sample holder. A schematic sketch of the sample holder is shown in Fig. 7. The tweezer points were gold plated to insure good ohmic contact to the sample and to prevent oxidation should water vapor condense on the probe. A thermometer was mounted on the outside

edge of the probe adjacent to the diode under test. The sample holder was mounted on the end of a 4-ft by 3/8-in.-diameter bakelite rod. The 4-ft rod allowed raising and lowering the sample into a liquid helium bath. Some of the samples were tested using a four-terminal probe to determine the effects of voltage drops at the ohmic contacts and in the leads. There was no difference in the diode characteristics as measured with this four-terminal probe or with the two-terminal tweezer probe.

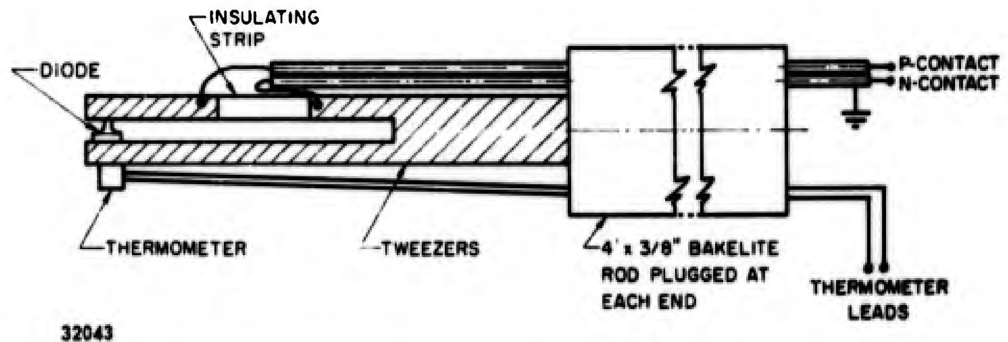

FIG. 7. SCHEMATIC SKETCH OF THE SAMPLE HOLDER.

The thermometer used to measure the temperature from 300 °K to 4.2 °K was a GaAs diode [Ref. 8]. The diode was forward biased with a current of 10^{-6} amp. The voltage across the diode at this bias varied with temperature as shown in Fig. 8. The thermometer was calibrated at 4.2, 77, 201, and 300 °K. A Leeds and Northrup K-3 bridge was used to measure the voltage. Using the straight-line approximation in Fig. 8, the temperature could be determined to the nearest 3 °K.

Electrical contact was provided to the sample through a three-wire system. Two coaxial wires were used. The centers were connected to the sides of the tweezers leading to the p and n sides of the sample. The shields were soldered together at both ends of the leads. This arrangement facilitated the capacitance measurements. The capacitance between the two center leads with the shields grounded at the bridge was 3.4 pf. This low capacitance allowed small-area, small-capacitance diodes to be accurately measured at the end of the 4-ft rod in the helium bath.

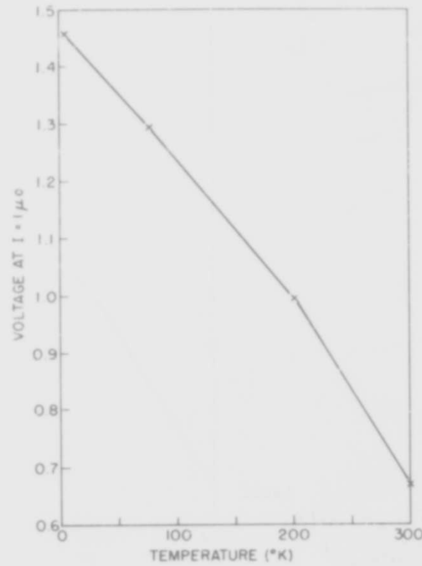

FIG. 8. THERMOMETER CALIBRATION AT $I_{diode} = 10^{-6}$ AMP.

A photograph of each sample was taken prior to testing. A typical photograph is shown in Fig. 9. The mesa is the round area in the general center of the square chip. Measurement of the distances d_1 and d_2

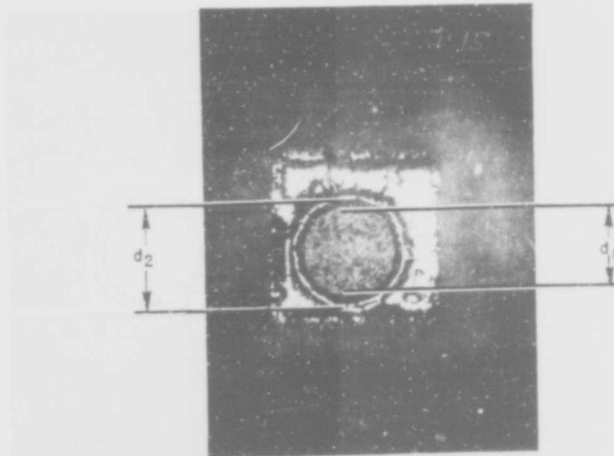

FIG. 9. PHOTOGRAPH OF A TYPICAL DIODE SHOWING METHOD OF MEASURING AREA.

allowed determination of the area of the top and base of the diode. The p-n junction is located between these two areas, with the area of the junction assumed to be the average of the two areas. For the large-area diodes the percentage error can be made small. Smaller diode areas can be found from capacitance-per-unit-area measurements made on the large-area diodes. The data taken on these diodes consisted of recording the forward I-V characteristics, the reverse I-V characteristics, and the capacitance-voltage relationship. The temperature range covered was from 4.2 °K to 300 °K and was continuously variable. The current measured ranged from 10^{-10} amp to 10^{-2} amp. The voltage seldom exceeded 12 v.

A schematic diagram of the test configuration used for recording I-V data is shown in Fig. 10. The current was measured using a Hewlett-Packard 425A microammeter. The voltage was measured with a John Fluke Model 825 differential voltmeter, a Hewlett-Packard 3440A digital voltmeter, or a Leeds and Northrup K-3 bridge. No essential changes were noticed when different meters were used. A 12-v storage battery was used as the power supply for most of the measurements.

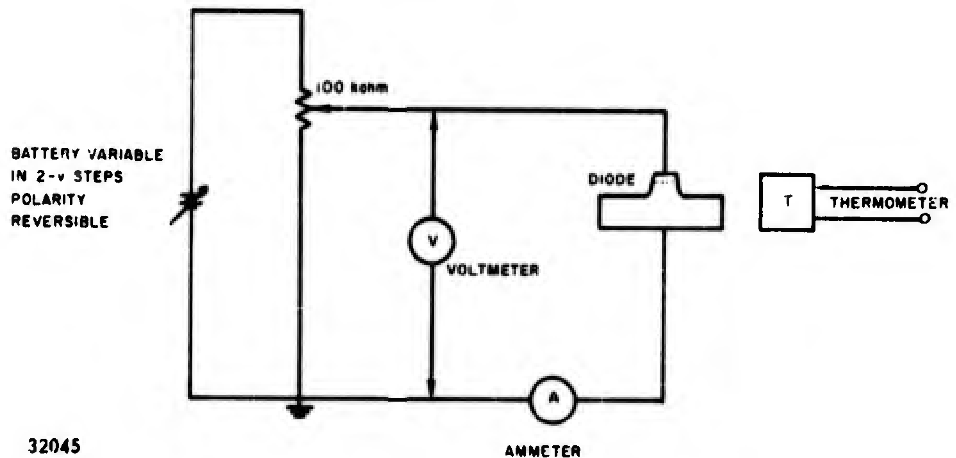

FIG. 10. SCHEMATIC OF I-V TEST CIRCUIT.

The capacitance vs voltage was measured using a Boonton 75A-S13 bridge. The limiting values of capacitance were determined by either the voltage available from the Boonton bridge or by the conductance of

the diodes. The capacitance of the diode was used in many cases to determine the area of the diode. This provided a useful technique for measuring small-area diodes where photographic techniques are somewhat inaccurate. The capacitance data provided information as to whether the junction was step or graded, as well as the value of the built-in voltage, and the width of the space-charge region of the diode.

C. EXPERIMENTAL DATA

The experimental data taken on these diodes consisted of recording the I-V characteristics and the capacitance vs voltage under forward and reverse bias at temperatures between 300 °K and 4.2 °K.

Typical plots of the forward log I-V data taken on four samples of various doping densities are shown in Figs. 11a-11d. The data shown for diode HPA-1 in Fig. 11a indicate the motivation for the work described in this paper. The currents at high temperature generally follow a characteristic of the form $\exp(qv/2kT)$ which is associated with normal thermal recombination. At low temperatures the characteristic has the form $\exp(\alpha v)$, where α is almost independent of temperature. This exponential characteristic will be shown to be consistent with an excess tunnelling current model.

Data similar to that shown in Fig. 11 were taken on all the diodes described in Table 1. The lightly doped samples tended to be dominated by thermal currents similar to the data presented in Fig. 11b. The low-temperature operating point of these lightly doped diodes was normally limited by carrier freeze-out and the appearance of double injection [Ref. 3]. Moderately doped samples had characteristics similar to those presented in Fig. 11a where the high-temperature current is thermal current and the low temperature current is tunnel current. Heavily doped samples such as that shown in Fig. 11c have currents dominated by tunnelling currents even at room temperature. Below 100 °K the appearance of band-to-band tunnelling appears at low voltages. In the most heavily doped sample shown in Fig. 11d, the tunnelling current to a deep trap is dominant at all temperatures below room temperature.

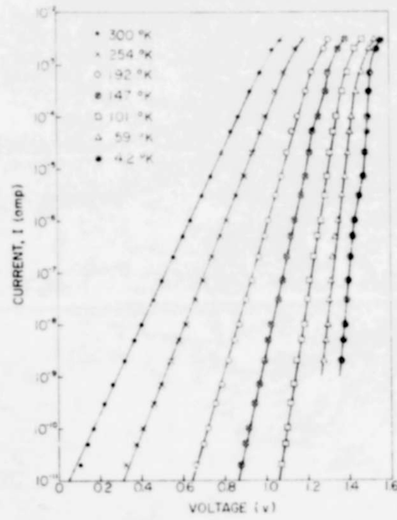

32046

a. HPA-1

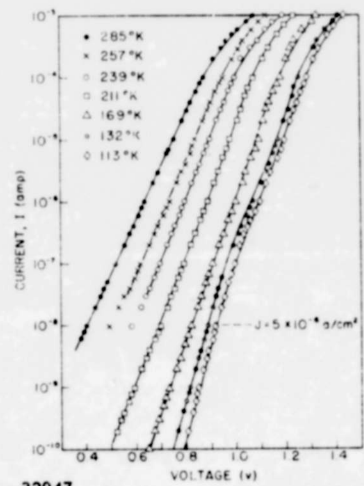

32047

b. D150

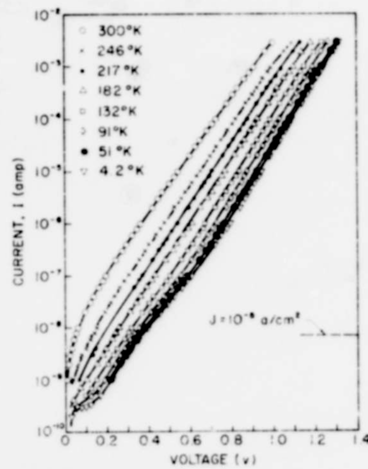

32048

c. D160

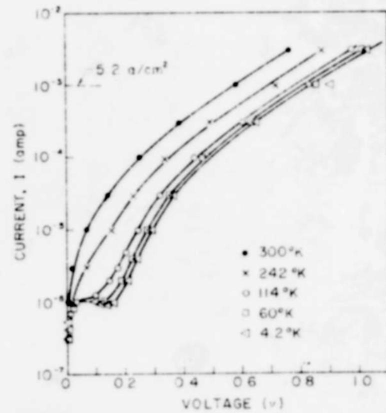

32049

d. D290

FIG. 11. PLOTS OF FORWARD I-V DATA ON FOUR SAMPLES OF VARIOUS DOPING DENSITIES.

The forward I-V data are partially summarized in Fig. 12. Here the forward current density for various samples is plotted as a function of applied voltage. Figure 12a represents the data at 300 °K and Fig. 12b represents the data at 4.2 °K. The data show the behavior of the tunnelling current at 4.2 °K as the doping density of the n-type parent is increased from 10^{17} cm^{-3} to $9.4 \cdot 10^{19}$ cm^{-3}. The data at 300 °K show similar effects for a somewhat wider range of doping densities. The wider range can be attributed to the inclusion in Fig. 12a of data on samples which were doped so lightly as to produce freeze-out of the carriers at 4.2 °K.

The reverse I-V characteristics of these diodes were also recorded as a function of temperature; they are summarized in Fig. 13 for two temperatures, 300 °K and 4.2 °K. As in Fig. 12, the effects of increased doping density are evident in the reverse I-V characteristics. These reverse characteristics are explained in terms of a band-to-band tunnelling model in Sec. C of Chapter IV.

All of the samples included in Table 1 do not appear in Figs. 11, 12, and 13. The diodes not included in these figures have data which are essentially redundant with data presented.

Typical capacitance-voltage data are presented in Fig. 14. The capacitance has been plotted as a function of applied voltage for different temperatures. These data can be used extensively in the analysis of the diode characteristics and will be discussed at some length in Chapter IV.

D. BULK-SURFACE CURRENT DETERMINATIONS

The currents that are reported here have been attributed to bulk current flow. To separate the bulk current from the surface current, the forward and reverse currents were measured by various methods as a function of diode area and perimeter. These methods, described below, support the conclusion that the measured current is bulk current.

1. In one method a fairly large area diode was produced. This diode was tested and etched to a smaller size. The testing and etching continued until the area of the diode became too small to be structurally stable. The ratio of initial to final area could be made

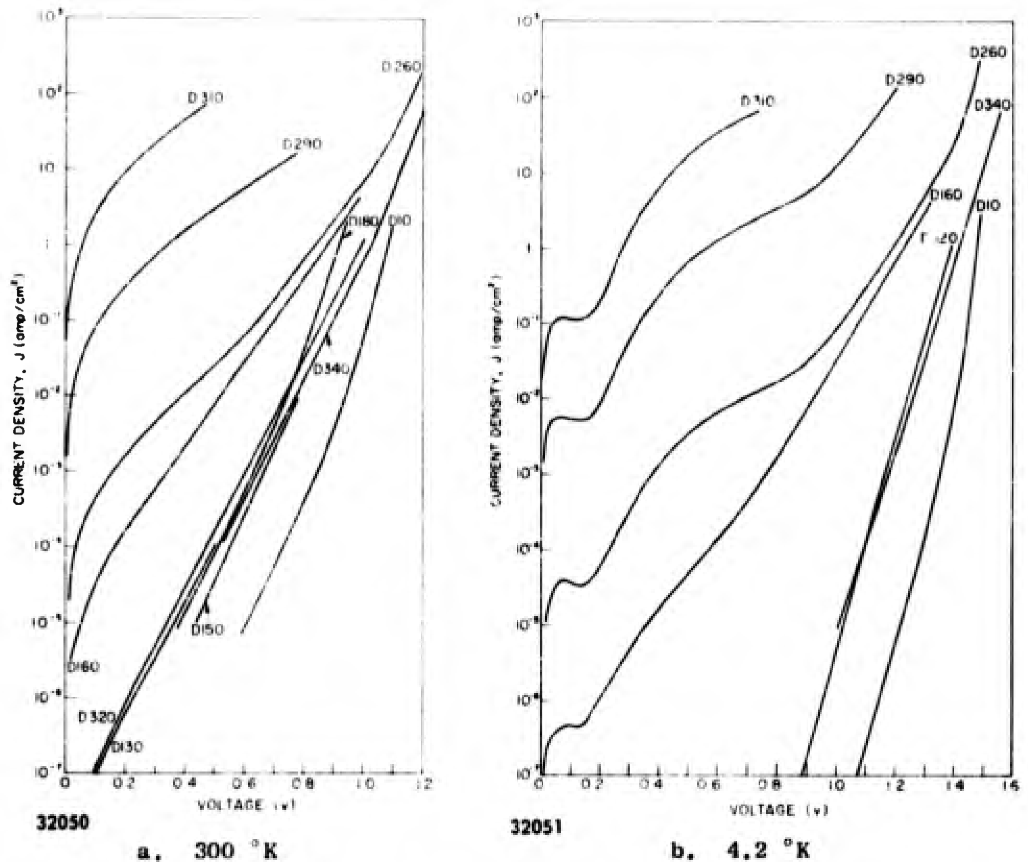

a. 300 °K b. 4.2 °K

FIG. 12. FORWARD I-V DATA ON ALL SAMPLES.

100:1, or greater, using this method, with a resulting perimeter ratio of 10:1. A typical plot of forward and reverse current as a function of applied voltage for successively smaller areas is shown in Fig. 15. These data were taken at 4.2 °K and 300 °K. It is readily apparent that the current "scales" with the diode area when the data are plotted as shown in Fig. 16. Here all area, perimeters, and currents have been normalized to the original values and the currents are seen to follow the areas rather than the perimeters.

2. The second method used to determine whether the measured current was surface or bulk current was to etch various-sized mesas from a chip and compare the current-voltage characteristics on a current-density basis. The results of this type of comparison were essentially the same as those found from the comparison shown in Figs. 15 and 16.

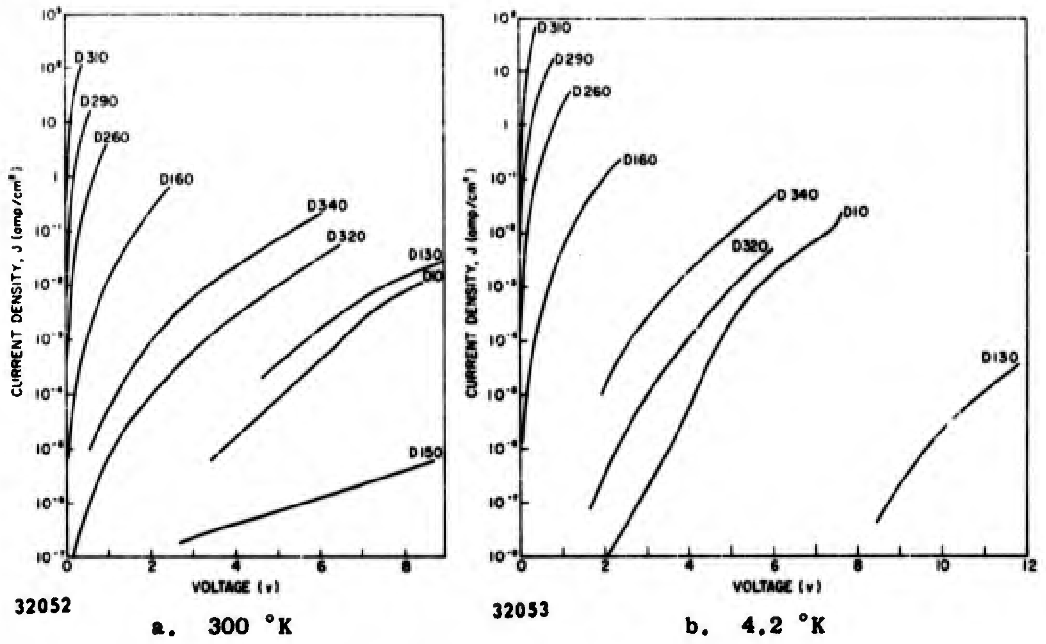

a. 300 °K b. 4.2 °K

FIG. 13. REVERSE I-V DATA ON ALL SAMPLES.

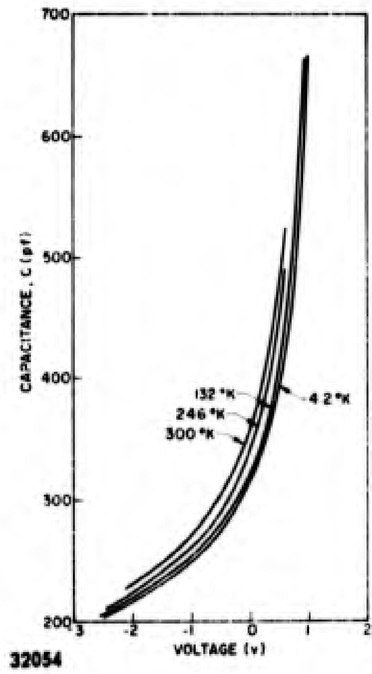

FIG. 14. CAPACITANCE VS VOLTAGE FOR DIODE D160.

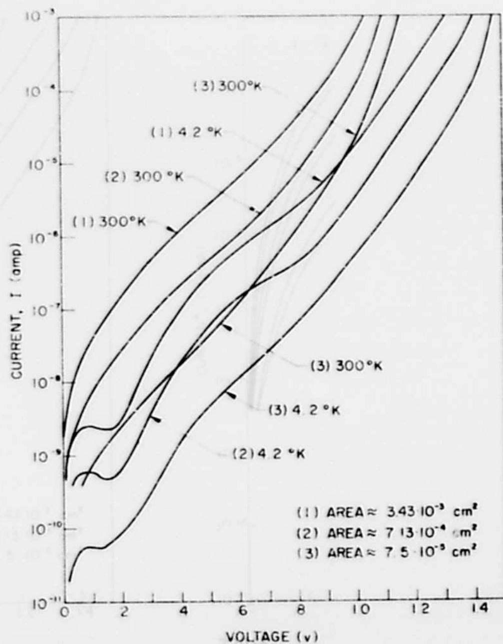

a. Forward

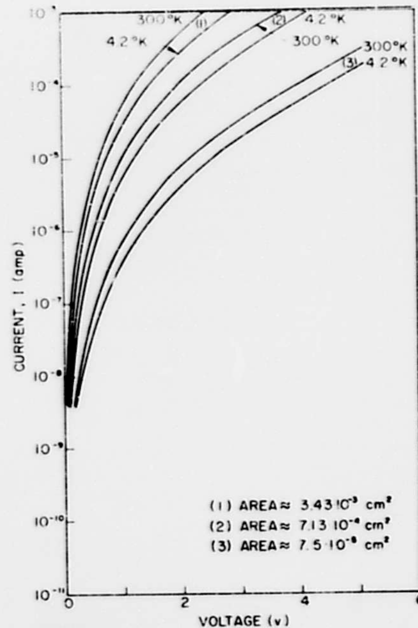

b. Reverse

FIG. 15. FORWARD AND REVERSE I-V CHARACTERISTICS AT 300 °K AND 4.2 °K FOR SUCCESSIVELY SMALLER AREAS OF DIODE D300.

3. A third type of measurement involving a guard-ring structure has been performed [Ref. 23]. This process was based on experiments in silicon which showed that some of the current varying as exp (qv/2kT) was associated with surface recombination [Ref. 24]. The high surface conductivity of the p-layer in GaAs has tended to confuse these results. In the one sample in which a surface current was reported [Ref. 23], a later experiment showed that when the guard-ring potential was reversed similar data were observed. Since the capacitance from center to ground on this structure was a function of guard-ring bias, the surface current, if present, was being masked by changes in diode current caused by variations in the space-charge region due to guard-ring bias.

The area-perimeter current measurements described in Figs. 15 and 16 are interpreted to indicate that the currents observed in these samples were bulk currents.

These comments concerning the area-perimeter currents should not be taken to imply that surface currents and nonuniform conduction were not observed. In many samples there was little or no correlation between

diode current and area or perimeter. None of the surface-current information was considered in the analysis presented here. All of the data presented and analyzed were taken from consistent sets of data obtained on at least three diodes from each diffusion run. The ratio of largest to smallest area was always greater than 30 and often was 100 or more.

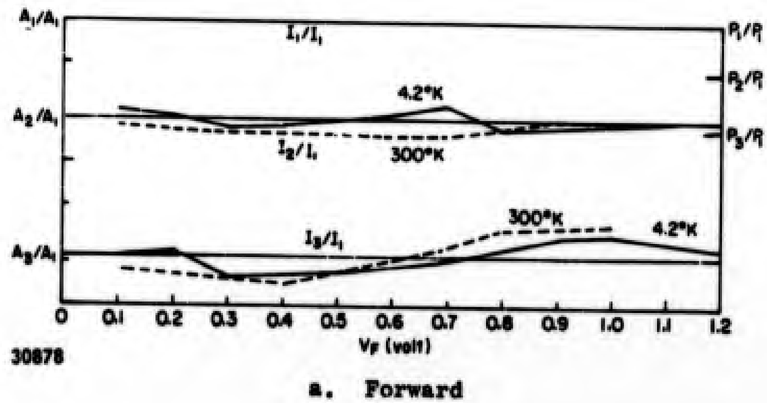

a. Forward

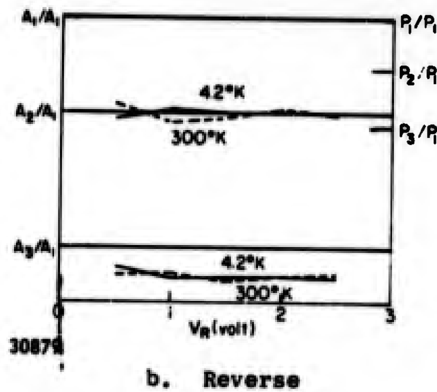

b. Reverse

FIG. 16. AREA-PERIMETER COMPARISON OF CURRENTS.

IV. ANALYSIS OF DATA

A. CAPACITANCE STUDIES

There is some question as to what value of built-in voltage should be used when calculating the tunnelling current. It has been pointed out earlier that the built-in voltage associated with the depletion region should be less than the band gap. The values of built-in voltage used in this paper to calculate the forward characteristics have been the experimentally determined values which are less than the band gap. A plot of C^{-2} vs V_a for diode D10 is shown in Fig. 17a for a step junction. A plot of C^{-3} vs V_a for diode EN-01 is shown in Fig. 17b for a graded junction. The built-in voltage is the zero intercept of these lines with the voltage axis. The built-in voltage vs temperature is plotted in Fig. 18 for a representative collection of step junctions and graded junctions. The theoretical band-gap variation with temperature is shown in these figures also. The measured built-in voltage is seen to be always less than the band gap, and increases as the temperature is lowered. The measured built-in voltage tends to vary slightly more than the band gap varies as the temperature is lowered. A table of built-in voltages at 4.2 °K and 300 °K is provided in Table 2 for both step and graded junctions. The grading constant a is also shown in the portion of the table applying to the graded junctions. The constant a has been evaluated at 300 °K and decreased only slightly as the temperature was lowered to 4.2 °K. In sample D150 in which carrier freeze-out occurred, the grading constant dropped drastically only below 82 °K.

The junction width can be determined from capacitance measurements as follows:

$$w = \epsilon A/C \tag{27}$$

The width of a typical junction, D160, vs applied bias is shown in Fig. 19. A common figure of merit for tunnel diodes is the width constant, defined as the width of the depletion region at one-volt total bias. The width constants for the diodes reported in this experiment are listed in Table 3 for 4.2 °K and 300 °K. The measured value of built-in voltage has been

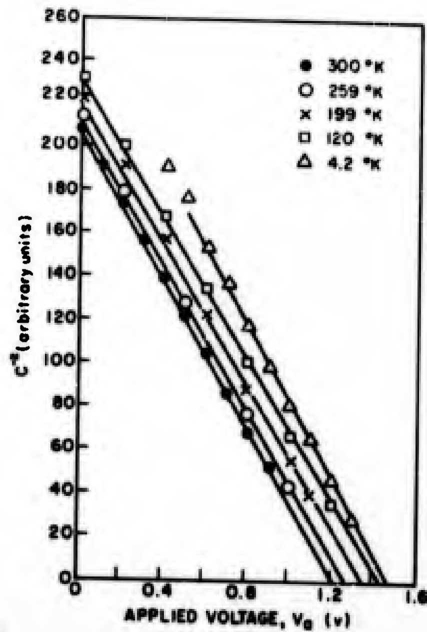

a. C^{-2} vs V_a for diode D10

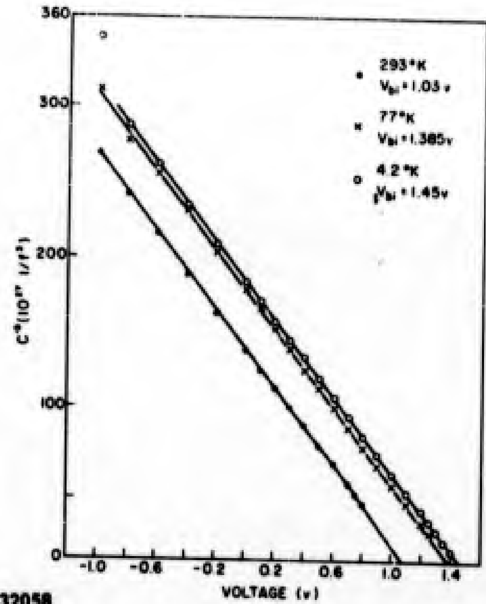

b. C^{-3} vs V_a for diode EN-01

FIG. 17. BUILT-IN VOLTAGE AS DETERMINED FROM CAPACITANCE DATA.

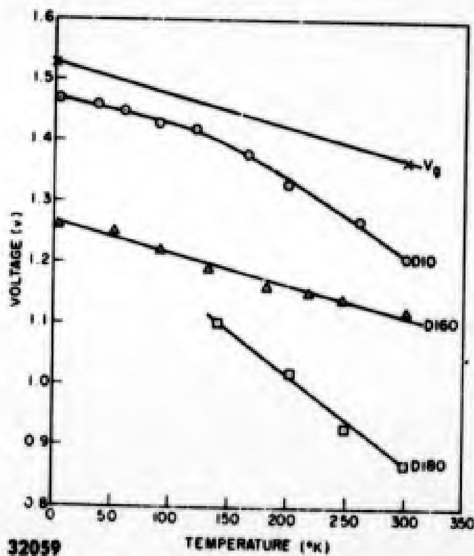

a. Step junctions

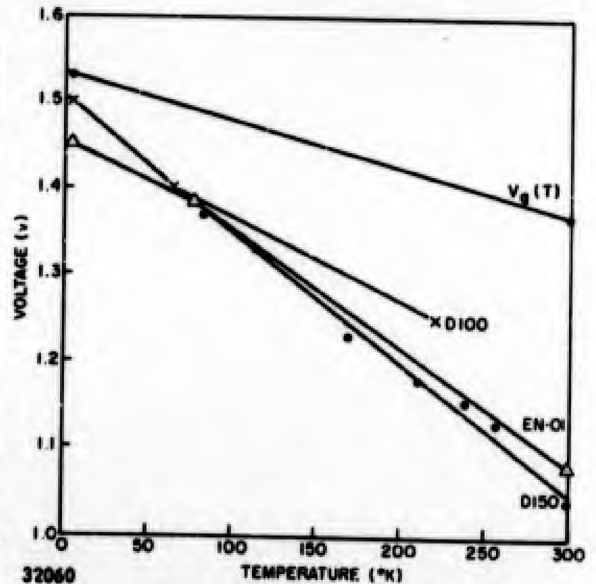

b. Graded junctions

FIG. 18. BUILT-IN VOLTAGE VS TEMPERATURE.

TABLE 2. BUILT-IN VOLTAGES AT 4.2 °K AND 300 °K

Diode	Built-in Voltage, V_{bi}		Grading Constant, a
	4.2 °K	300 °K	
Graded Junctions			
EN-01	1.45 v	1.08 v	$1.43 \cdot 10^{23}$ cm^{-4}
HPA-1	Cap	Cap	Cap
D100	1.50	1.40	$3.8 \cdot 10^{22}$ cm^{-4}
D130	CF	Cap	Cap
D150	CF	1.04	$9 \cdot 10^{20}$ cm^{-4}
D260	1.37	1.02	$3.18 \cdot 10^{22}$ cm^{-4}
D300	1.50	1.20	--
Step Junctions			
D10	1.47	1.21	
D160	1.26	1.12	
D180	CF	0.90	
D290	Con	Con	
D310	Con	Con	
D320	1.43	1.20	
D340	1.40	1.20	
D350	1.47	1.22	
D380	1.25	1.14	

CF - carrier freeze-out at low temperatures.
Con - high conductance did not allow sufficient capacitance data.
Cap - low capacitance due to wide space-charge region.

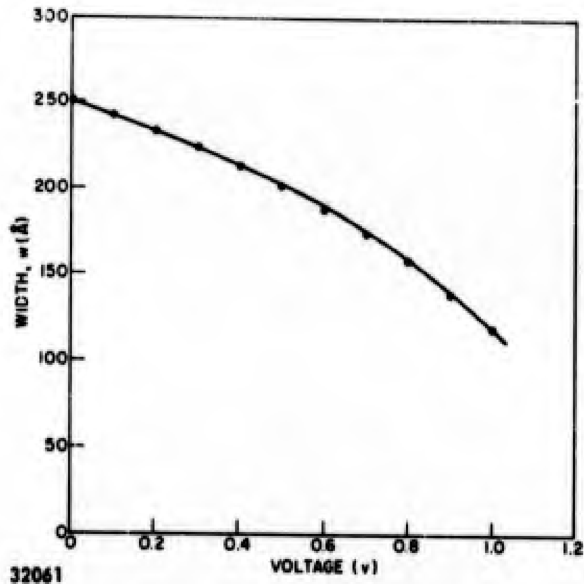

FIG. 19. JUNCTION WIDTH AT 4.2 °K VS APPLIED VOLTAGE FOR DIODE D160.

used to determine the width constant. The diodes with lowest width constants show the greatest conduction at 4.2 and 300 °K, which is indicated by comparing Table 3 with Fig. 12. The width constants rise somewhat as the temperature is lowered, probably a consequence of the rising band gap. The width constants have not been calculated for the diodes which displayed thermal currents at 300 °K.

The capacitance data yield an indication of the effects of compensation in the junction region. The probable cause of this compensation has been assumed to be the in-diffusion of copper during the zinc diffusion process [Ref. 25]. In terms of the capacitance at zero applied bias, the carrier concentration of the lightly doped side of a step junction can be found from Eq. (26b) as

$$N_D = \frac{2V_{bi}\, C^2}{q\, \epsilon\, A^2} \tag{28}$$

A plot of C/A (0 v, 300 °K) and C/A (0 v, 4.2 °K) as a function of N_D is shown in Fig. 20 along with the value predicted using $V_{bi} = V_g$.

TABLE 3. WIDTH CONSTANTS AT 4.2 °K AND 300 °K

Diode	Width Constant (Å)	
	4.2 °K	300 °K
EN-01	875	Thermal current
D10	780	Thermal current
D100	1900	Thermal current
D130	Carrier freeze-out	Thermal current
D150	Carrier freeze-out	Thermal current
D160	228	211
D180	Carrier freeze-out	Thermal current
D260	286	220
D290	215	210
D300	429	415
D310	180	170
D320	945	925
D340	760	Thermal current
D350	1610	Thermal current
D380	350	240

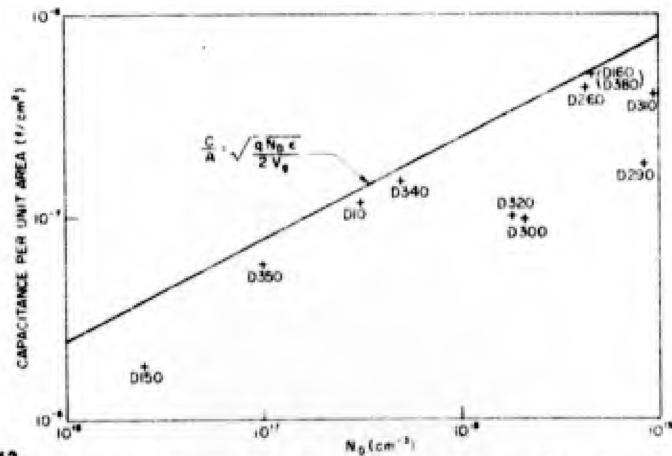

32062

FIG. 20. CAPACITANCE PER UNIT AREA VS DOPING DENSITY FOR A STEP JUNCTION.

The values predicted by Eq. (28) at 300 °K and 4.2 °K are almost identical and thus one line in Fig. 20 is used to show the situation at 4.2 and 300 °K. The value of N_D chosen for the experimental values in Fig. 20 is the value of N_D of the parent. All of the samples are seen to have an experimental value of C/A which is lower than the predicted values. This low value of C/A suggests that the material is compensated in the junction region. A comparison of N_D (parent), N_D (C/A), and the degree of compensation N_D (parent) minus N_D (C/A) is presented in Table 4. The tendency is for the more heavily doped samples to be more heavily compensated. The values of compensation given in Table 4 scatter around one-half the value of the doping of the parent. Thus the compensation could be the zinc diffusion front extending into the n-type material. This would be compatible with the fact that the junction starts when $N_D = N_A$, or when the material is exactly compensated.

A typical plot of N_D as a function of temperature as determined from capacitance measurements and experimentally determined values of V_{bi} is shown in Fig. 21. These data are typical of all of the samples in which carrier freeze-out did not occur and which remained conducting at 4.2 °K.

B. FORWARD CHARACTERISTICS

In this section the forward characteristics are discussed and analyzed. The exponential behavior of the low-temperature current for step junctions is compared to the theoretical tunnelling predictions. The general forward characteristics are compared with the theoretical predictions and the effective tunnelling masses are obtained. The effective tunnelling masses vary with temperature and doping density in a reasonable manner. The recombination probability is obtained and is seen to increase with increasing temperature.

The forward-tunnelling current has been described in terms of the doping density of a step junction by Eq. (21a). The tunnelling current in a step junction has an exponential voltage dependence of the form $I = I_1 \exp(\alpha V_a)$, where α is given by Eq. (22b). The graded junction has a voltage dependence of the form $I = I_2 \exp\left[\beta(V_{bi} - V_a)^{5/6}\right]$ which is almost

TABLE 4. DEGREE OF COMPENSATION IN THE JUNCTION REGION

Diode	N_D (parent) (cm^{-3})	N_D (C/A) (cm^{-3})	Degree of Compensation* (cm^{-3})
D10	$3.1 \cdot 10^{17}$	$2.4 \cdot 10^{17}$	$7 \cdot 10^{16}$
D150	$2.5 \cdot 10^{16}$	$6.3 \cdot 10^{15}$	$1.9 \cdot 10^{16}$
D160	$4.6 \cdot 10^{18}$	$3.2 \cdot 10^{18}$	$1.4 \cdot 10^{18}$
D260	$4.3 \cdot 10^{18}$	$3.4 \cdot 10^{18}$	$9 \cdot 10^{17}$
D290	$8.3 \cdot 10^{18}$	$3.2 \cdot 10^{18}$	$5.1 \cdot 10^{18}$
D300	$2.1 \cdot 10^{18}$	$4.0 \cdot 10^{17}$	$1.7 \cdot 10^{18}$
D310	$9.4 \cdot 10^{18}$	$2.7 \cdot 10^{18}$	$4.7 \cdot 10^{18}$
D320	$1.8 \cdot 10^{18}$	$3.3 \cdot 10^{17}$	$1.5 \cdot 10^{18}$
D340	$5 \cdot 10^{17}$	$3.8 \cdot 10^{17}$	$1.2 \cdot 10^{17}$
D350	$1 \cdot 10^{17}$	$6.8 \cdot 10^{16}$	$3.2 \cdot 10^{16}$

*Copper solubility in GaAs at 900 °C is between $3 \cdot 10^{17}$ and 10^{18} cm^{-3} [Ref. 25].

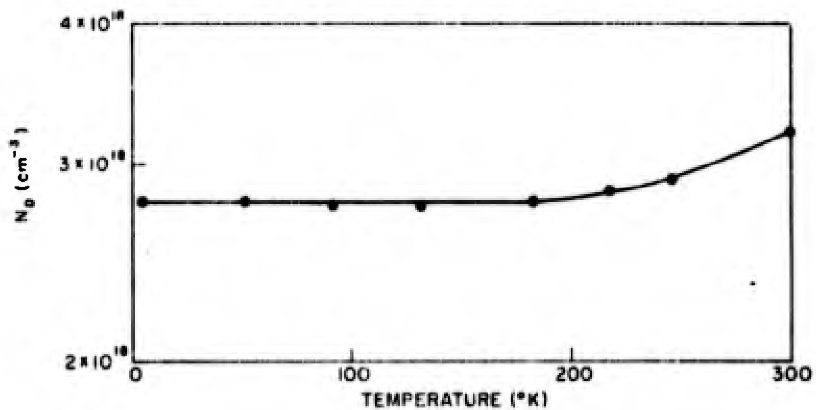

32063

FIG. 21. PLOT OF N_D VS TEMPERATURE FOR DIODE D160.

exponential in applied voltage. The recombination probability has been assumed to be only a weak function of voltage, which is certainly not always true.

The slopes of the forward log I-V characteristics for the step junctions tested have been compared with the slope as given by Eq. (22b). This comparison is shown in Fig. 22 where the slope of the log I-V characteristic at 4.2 °K is plotted against N_D at 4.2 °K. Two theoretical curves are presented, one applying to the average field approximation and the other applying to the maximum field approximation. The observed slopes are seen to agree with the maximum field approximation. The two doping densities associated with each sample are the doping density of the parent and the doping density determined from capacitance measurements.

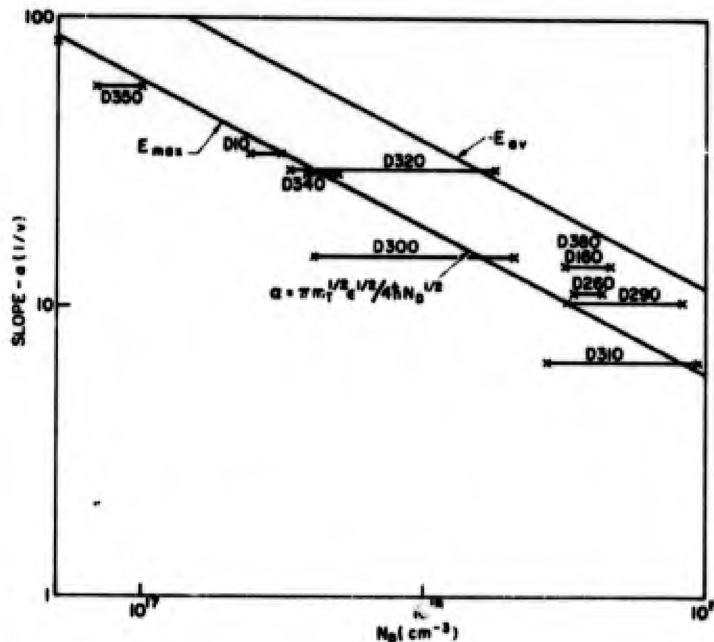

31508

FIG. 22. SLOPE OF LOG I-V CHARACTERISTIC VS DOPING DENSITY.

The effective tunnelling mass can be estimated from the measured diode capacitance, area, and I-V characteristic. For a diode (step, graded, or some general junction shape), the tunnelling characteristic has been

given by Eq. (19). Under the assumption that the recombination probability is relatively independent of energy, a plot of log J vs $\left[(V_{bi} - V_a)^{1/2} A/C\right]$ should be a straight line of slope

$$\text{slope} = \frac{\pi\, m_T^{1/2}\, q^{1/2}\, \epsilon}{4\sqrt{2}\, \hbar} \tag{29}$$

From the slopes of these plots the effective mass can be determined as

$$m_T = \frac{32\, \hbar^2\, (\text{slope})^2}{\pi^2\, q \epsilon^2} \tag{30}$$

Plots of log J vs $(V_{bi} - V_a)^{1/2}$ A/C are shown in Fig. 23 for temperatures T = 4.2 °K and T = 300 °K respectively. From these slopes the effective masses shown in Table 5 have been calculated. In some cases, such as D260, the recombination probability P_R varied appreciably with voltage. The best fit to the straight-line portion of the plot has been used to calculate the tunnelling mass. A discussion of the variation of P_R with voltage follows later in this section. In plotting Figs. 23a and 23b the measured values of V_{bi} were used. At 300 °K the nonthermal currents are the only currents that have been analyzed.

There has been a tendency for the more heavily doped samples to have a higher effective tunnelling mass. This is demonstrated in Fig. 24, where the effective tunnelling mass is plotted as a function of doping density of the parent. If the mass is given by an equation of the form

$$m = \frac{\hbar^2}{\partial^2 \mathcal{E}/\partial k^2} \tag{31}$$

then this would imply that the conduction band has a less than parabolic shape as the impurity density is increased. Similar increases in conduction mass with increased doping density in GaAs have been observed [Ref. 26].

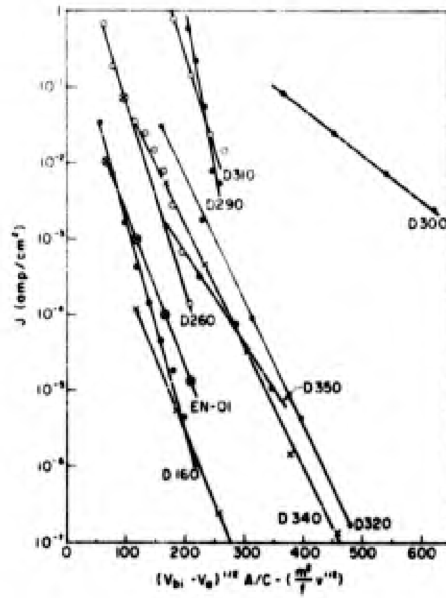

32064

a. T = 4.2 °K

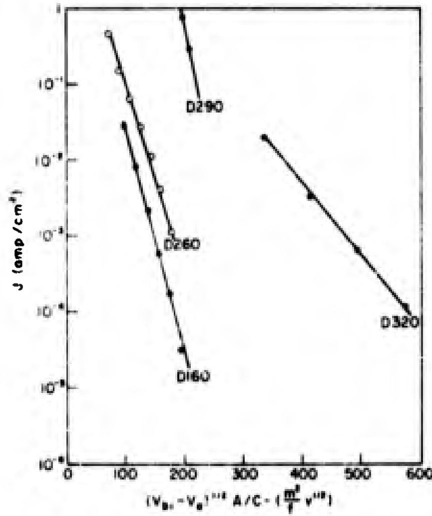

32065

b. T = 300 °K

FIG. 23. PLOTS OF LOG J VS $(V_{bi} - V_a)^{1/2}$ A/C.

TABLE 5. EFFECTIVE TUNNELLING MASSES AT T = 4.2 °K and 300 °K AS DETERMINED FROM THE FORWARD I-V CHARACTERISTICS

Diode	Effective Tunnelling Mass, m_T		Dopant of Parent (cm^{-3})
	4.2 °K	300 °K	
D10	0.04 m_o	Thermal current	$3.1 \cdot 10^{17}$
D160	.079 m_o	0.088 m_o	$4.6 \cdot 10^{18}$
D260	.068 m_o	0.068 m_o	$4.3 \cdot 10^{18}$
D290	.188 m_o	0.160 m_o	$8.3 \cdot 10^{18}$
D300	.004 m_o	Very low	$2.1 \cdot 10^{18}$
D310	.068 m_o	Con	$9.4 \cdot 10^{18}$
D320	.030 m_o	0.011 m_o	$1.8 \cdot 10^{18}$
D340	.032 m_o	Thermal current	$5.0 \cdot 10^{17}$
D350	.017 m_o	Thermal current	$1.0 \cdot 10^{17}$
EN-01	.047 m_o	--	$2.0 \cdot 10^{17}$

Con - conductance too high at 300 °K to measure capacitance accurately.

The effective tunnelling mass has been measured as a function of temperature. In a sample in which the temperature dependence of m_T was measured in the forward direction the mass increased as the temperature was increased. These data are presented in Fig. 25 for sample D160. This increase is seen to correlate with the increase in effective mass observed in conduction effective mass [Ref. 26]. Tiemann and Fritzsche [Ref. 27] have indicated that the temperature dependence of the reduced effective tunnelling mass is nearly proportional to the band-gap change, but about four times smaller than the temperature dependence of the band gap. Using the measured values of built-in voltage applying to sample D160, we have at T = 4.2 °K, V_{bi} = 1.26 v, $m_T = 0.08\ m_o$; and at T = 300 °K, V_{bi} = 1.12 v, $m_T = 0.09\ m_o$. Thus

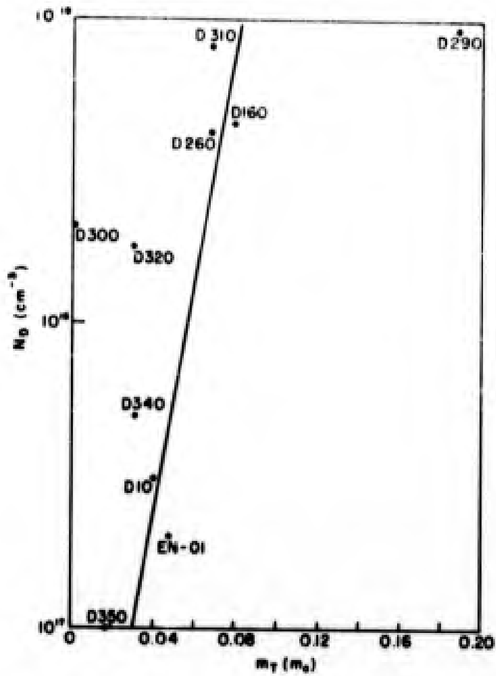

32066

FIG. 24. EFFECTIVE TUNNELLING MASS FOR VARIOUS DOPING DENSITIES OF THE PARENT AS DETERMINED FROM FORWARD I-V CHARACTERISTICS.

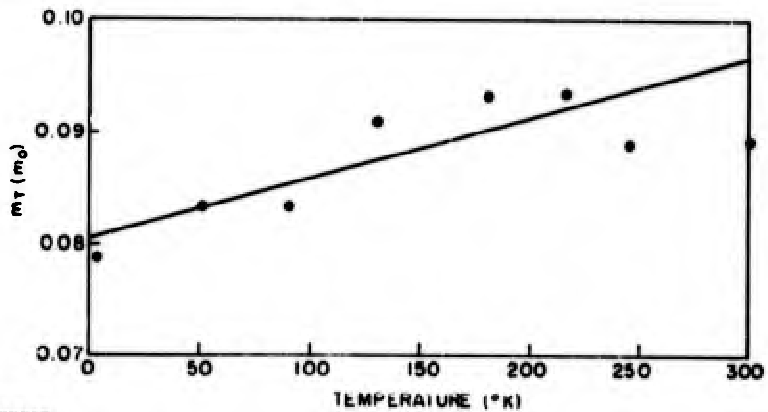

32067

FIG. 25. TEMPERATURE DEPENDENCE OF EFFECTIVE TUNNELLING MASS AS OBTAINED FROM FORWARD CHARACTERISTICS.

$$\frac{\Delta m_T}{m_T} = 0.111$$

and

$$\frac{\Delta \mathcal{E}_g}{\mathcal{E}_g} = 0.116$$

The measured temperature variation yields

$$\frac{\Delta \mathcal{E}_g}{\mathcal{E}_g} \approx \frac{\Delta m_T}{m_T}$$

which is somewhat larger than the value of

$$\frac{1}{4}\frac{\Delta \mathcal{E}_g}{\mathcal{E}_g} = \frac{\Delta m_T}{m_T}$$

predicted in Ref. 27.

At this point it is possible to compare the magnitudes of the forward currents as predicted on a tunnelling basis with those observed experimentally. The recombination probability, defined as the ratio of the measured current to the forward current, is used for this comparison. A recombination probability less than unity indicates measured currents that are less than the calculated values. In a band-to-trap-to-band tunnelling model the recombination probability is associated with the trap condition and trap density involved in the tunnelling process. The magnitude of the recombination probability is an indication of the trap density, and the temperature dependence is an indication of the end state changes with temperature. The measured excess tunnelling current has been compared with the tunnelling current that would be calculated on the basis of Eq. (19). The incident current has been given by Eq. (13), where N_D and $\overline{U}$ are associated with the values measured from capacitance studies.

The tunnelling probability has been calculated using the measured values of capacitance, area, built-in voltage, and tunnelling mass. The recombination probability is plotted in Fig. 26 as a function of applied bias at 4.2 °K for various samples. Most of the samples have a recombination probability that is relatively independent of energy. Sample D260 is seen to have a high recombination probability in the vicinity of $V_a = 0.4$ to 0.6 v. This high recombination probability may be tunnelling to a high density of deep traps such as copper, or to traps introduced by the zinc diffusion front. The low values of recombination probability indicate measured currents much lower than predicted by Eq. (19).

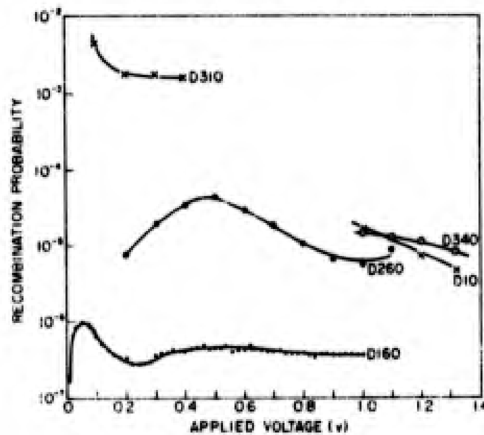

32068

FIG. 26. RECOMBINATION PROBABILITY AS A FUNCTION OF APPLIED BIAS.

The recombination probability increased as temperature increased. A plot of P_R for temperatures between 4.2 and 300 °K is shown in Fig. 27 for sample D160. This temperature dependence is almost independent of applied bias in this sample. The temperature dependence of the recombination probability fits an exponential increase with temperature of the form

$$P_R = P_R(T = 0\ ^\circ K)\ \exp\ (\gamma T) \tag{32}$$

where $P_R(T = 0\ ^\circ K) = 3.6 \cdot 10^{-7}$ and $\gamma = 1.15 \cdot 10^{-2}/^\circ K$.

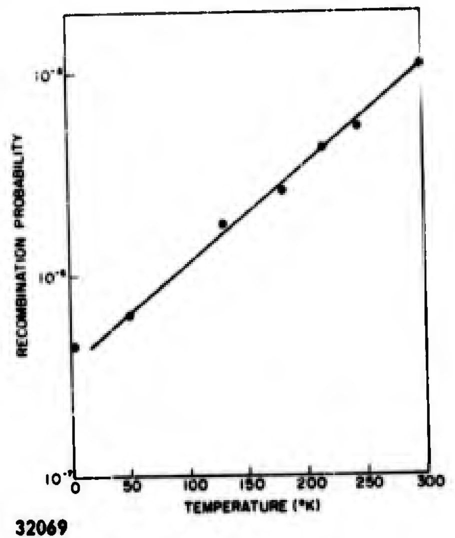

FIG. 27. RECOMBINATION PROBABILITY VS TEMPERATURE FOR DIODE D160 AT V_a = 0.6 v.

C. REVERSE CHARACTERISTICS

In this section the reverse I-V characteristics are compared with those predicted from a band-to-band tunnelling model. The functional form of the reverse I-V characteristic is compared with the experimental data and the effective masses are found for each sample for which an effective mass could be calculated. The effective masses are seen to vary with doping density of the parent and with temperature. The magnitudes of the reverse tunnelling current are compared with the magnitudes observed at 4.2 °K.

The reverse tunnelling current should have a characteristic that is given by Eq. (25). If the junction area is measured photographically and the capacitance-voltage characteristic is known, then this characteristic can be compared directly with the measured results.

The reverse currents have the functional form of tunnelling currents. This form can be seen by plotting

$$\log \frac{J}{[V_a \, C(V_g + V_a)/A]} \quad \text{vs} \quad \left[\frac{C(V_g + V_a)}{A}\right]^{-1}$$

This plot is shown in Figs. 28a and 28b for temperatures of $T = 4.2\ ^\circ K$ and 300 °K. These plots should have slopes given by

$$\text{slope} = \frac{\pi\, m_T^{1/2}\, g^{1/2}\, V_g^{3/2}\, \epsilon}{4\sqrt{2}\,\hbar} \tag{33}$$

where $V_g = 1.53$ v at 4.2 °K, and 1.37 v at 300 °K. The results of Fig. 28 are seen to have the functional form predicted by Eq. (25). The effective tunnelling mass can be found from the slopes of these plots by noting that

$$m_T = \frac{32\,\hbar^2\,(\text{slope})^2}{\pi^2\, q\, V_g^3\, \epsilon^2} \tag{34}$$

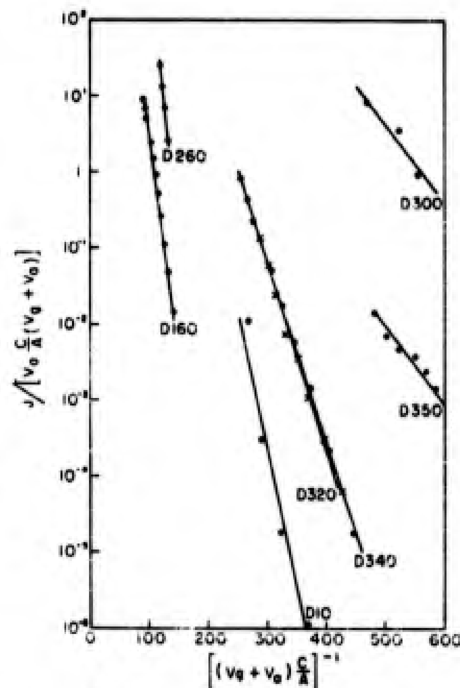

a. T = 4.2 °K

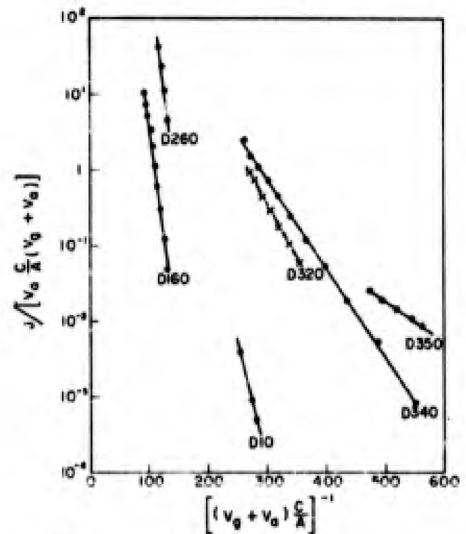

b. T = 300 °K

FIG. 28. PLOTS OF LOG $J/[V_a\ C/A\ (V_g + V_a)]$ VS $[C/A\ (V_g + V_a)]^{-1}$.

Table 6 shows the effective tunnelling masses as determined from the slopes of the reverse characteristics. These values tend to scatter around the reduced hole-electron mass of 0.063 m_o. There is general agreement between the values given in Table 5 found from the forward characteristics and the values given in Table 6 found from the reverse characteristics. There is a tendency for the heavily doped samples to have a higher effective tunnelling mass. A plot of the effective tunnelling mass vs doping density of the parent at 4.2 °K is shown in Fig. 29.

The effective mass tends to increase as the temperature increases from 4.2 to 300 °K. An increase in conduction mass has been observed in GaAs with increasing temperature [Ref. 26]. The temperature dependence of effective tunnelling mass of diodes D160 and D260 is plotted in Fig. 30 for temperatures between 4.2 and 300 °K. The increase shown in Fig. 30 is considered to be in qualitative agreement with the predictions of Tiemann and Fritzsche [Ref. 27] but, as in the case of the forward currents, the temperature dependence of the tunnelling mass is higher than their estimates.

In the most heavily doped samples, diode conductance limited the range over which capacitance-voltage data could be taken. If a step junction is assumed, then the functional form for capacitance can be substituted into Eq. (25) with the result that a plot of

$$\log\left[\frac{J}{V_a(V_g + V_a)^{1/2}}\right] \quad \text{vs} \quad (V_g + V_a)^{-1/2}$$

should yield a straight line. Plots of this form are shown in Fig. 31 for the data taken at 4.2 °K and 300 °K on the two most heavily doped samples, D290 and D310. Since the theoretical slope of this line is not accurately known, the effective tunnelling mass cannot be extracted with the accuracy that it is when determined from Figs. 28a and 28b. The functional form of the current is seen to follow the tunnelling model.

TABLE 6. EFFECTIVE TUNNELLING MASS AS DETERMINED FROM REVERSE I-V CHARACTERISTICS AT 4.2 °K AND 300 °K

Diode	Effective Mass, m_T		Doping of Parent (cm^{-3})
	4.2 °K	300 °K	
D10	$0.030\ m_o$	$0.0377\ m_o$	$3.1 \cdot 10^{17}$
D130	CF	Cap	$6.1 \cdot 10^{15}$
D150	CF	Cap	$2.5 \cdot 10^{16}$
D160	$0.099\ m_o$	$0.123\ m_o$	$4.6 \cdot 10^{18}$
D180	CF	Cap	$3.1 \cdot 10^{17}$
D260	$0.088\ m_o$	$0.118\ m_o$	$4.3 \cdot 10^{18}$
D290	Con	Con	$8.3 \cdot 10^{18}$
D300	$0.008\ m_o$	$0.0005\ m_o$	$2.1 \cdot 10^{18}$
D310	Con	Con	$9.4 \cdot 10^{18}$
D320	$0.0205\ m_o$	$0.0079\ m_o$	$1.8 \cdot 10^{18}$
D340	$0.0183\ m_o$	$0.0053\ m_o$	$5.0 \cdot 10^{17}$
D350	$0.0015\ m_o$	---	$1.0 \cdot 10^{17}$

CF - carrier freeze-out at low temperatures.

Con - capacitance measurements limited by high conductance.

Cap - low capacitance due to wide space-charge region.

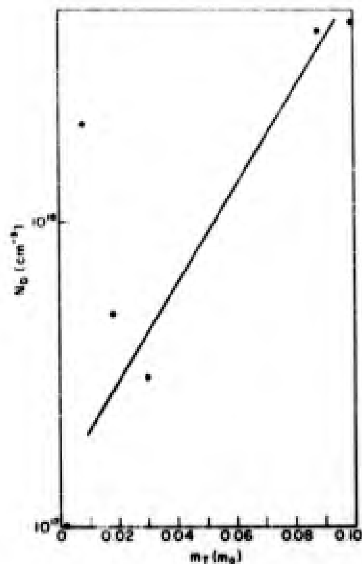

32072

FIG. 29. EFFECTIVE TUNNELLING MASS FOR VARIOUS DOPING DENSITIES OF THE PARENT AS DETERMINED FROM REVERSE I-V CHARACTERISTICS.

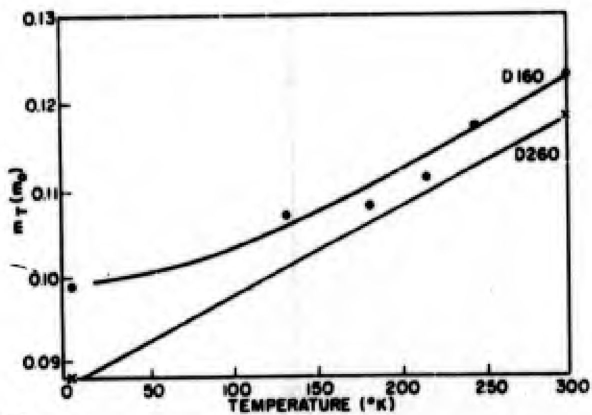

32073

FIG. 30. TEMPERATURE DEPENDENCE OF EFFECTIVE TUNNELLING MASS AS OBTAINED FROM REVERSE CHARACTERISTICS.

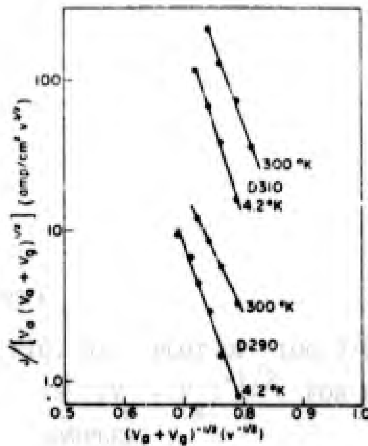

32074

FIG. 31. PLOT OF LOG $J/[V_a(V_a + V_g)^{1/2}]$ VS $(V_a + V_g)^{-1/2}$ FOR HEAVILY DOPED SAMPLES.

A comparison of the magnitudes of the currents predicted by Eq. (25) with those values measured has been made at 4.2 °K and is plotted in Fig. 32. The maximum field approximation has been used in calculating the theoretical curves of Fig. 32. The reduced hole-electron mass of $m_T = 0.063\ m_o$ has also been used. The step-junction approximation has been used and only the experimental data applicable to step junctions are shown. The measured values of I-V data are considered to be in good agreement with the predicted values. The description of the various sample parameters is shown in Table 4. The two doping densities given in this table are used to describe the doping densities of the sample discussed in Fig. 32.

D. LOW-BIAS CHARACTERISTICS

It has been pointed out* that for small positive and negative biases the I-V characteristics should be nearly linear. The forward and reverse currents should also be almost identical. This would be evident from a power series expansion of the expressions for tunnelling current about zero volts. Temperature and density-of-states expressions have not been included in the calculations of Chapter II and thus more exact calculations are needed to determine the low-bias expansions accurately.

*W. Shockley, private communication.

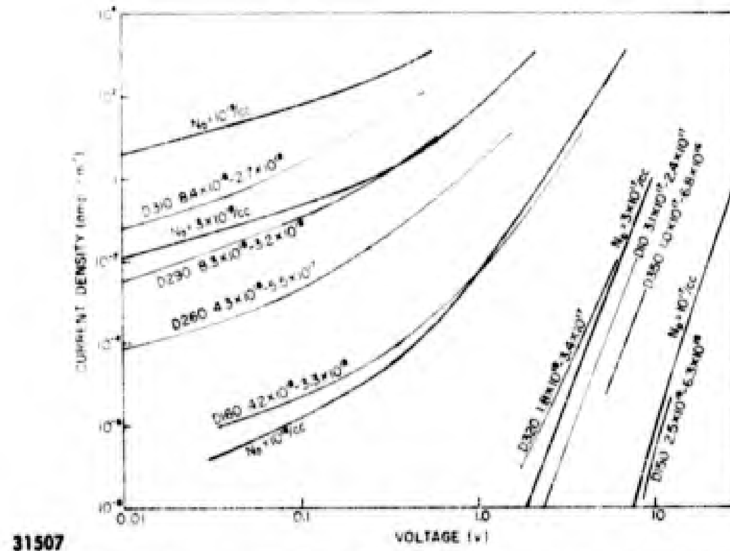

31507

FIG. 32. REVERSE TUNNELLING CURRENT VS APPLIED VOLTAGE AT $T = 4.2$ °K.

An expansion of the characteristics of tunnel diodes, including temperature and density-of-states effects at low voltages, has been carried out by Bates [Ref. 28]. The assumptions leading to his result involve high-temperature approximations and may not be valid below 100 °K; but for temperatures above 100 °K, the low-voltage expansion becomes

$$I = -B \frac{1 - \exp\left(\frac{qV}{kT}\right)}{\beta + 1 + \exp\left(\frac{qV}{hT}\right)} \tag{35}$$

where B and β are constants involving band gap, Fermi levels, and temperature. The low-voltage expansion for $V \ll kT/q$ becomes

$$I \approx \lambda V - \lambda' V^2 + \dots \tag{36}$$

where λ and λ' are new constants involving B, β, and kT/q. At fixed bias the reverse current will be slightly greater than the forward current. A typical low-voltage I-V characteristic is shown in Fig. 33 for diode D310 at 77 °K and 300 °K. These data have been plotted as

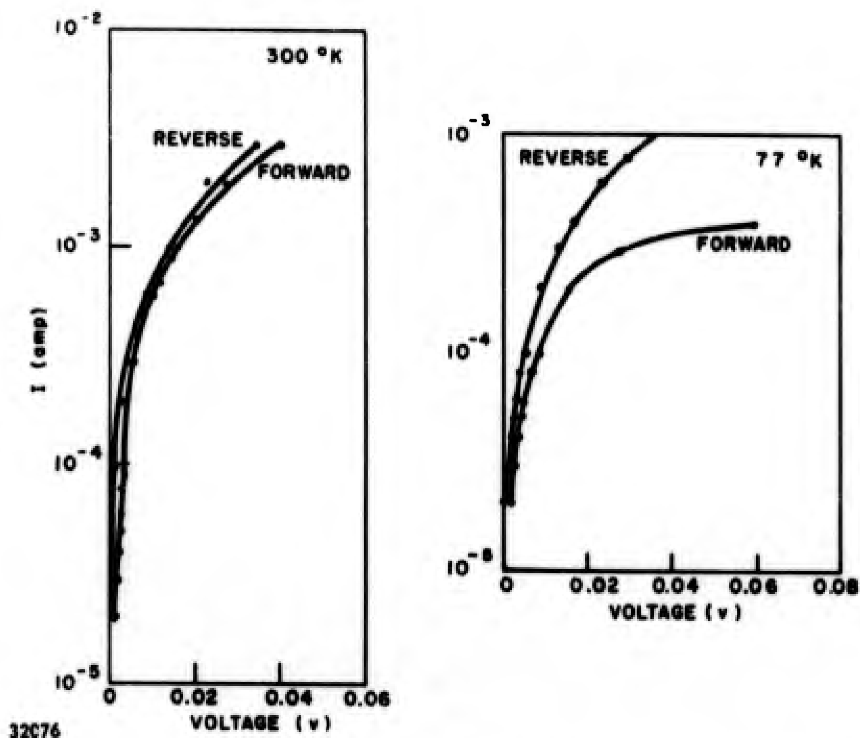

FIG. 33. LOW-LEVEL TUNNELLING CURRENTS AT 300 °K AND 4.2 °K.

log I - log V plots as shown in Fig. 34. This figure also includes some data taken on diode D290 at 4.2 °K. Figures 33 and 34 show that the reverse current is somewhat higher than the forward current around zero volts. All of the curves shown in Fig. 34 are superlinear with characteristics given by $I = V^n$, where $1.13 < n < 1.65$. The slight departure from linearity is considered to be in good agreement with Eq. (36). The power n is also slightly greater in the reverse direction than in the forward direction, which is to be expected.

E. HIGH-TEMPERATURE EFFECTS

The thermal currents dominate the high-temperature forward characteristics of the more lightly doped samples. These characteristics are analyzed below in terms of a lifetime and a diffusion length. The lifetime appears to be that of holes in n-type material, and the diffusion

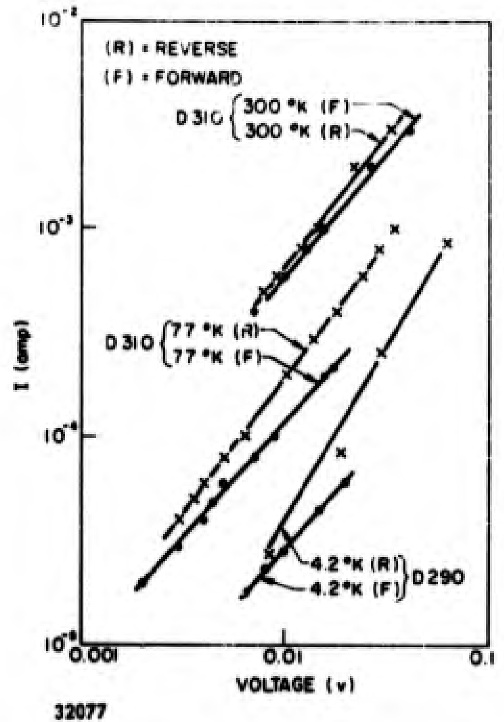

FIG. 34. LOG I - LOG V FOR LOW-VOLTAGE TUNNELLING CURRENT.

length is the hole diffusion length in n-type material. The values of lifetime and diffusion length found here are in agreement with existing accepted values, but the values measured here should be understood to mean no more than agreement with existing work.

If the forward current is due to recombination in the space-charge region, then the current should have a characteristic of the form [Ref. 2]

$$I = \frac{kT}{q} \frac{qn_i A}{E\tau} \exp\left(\frac{qv}{2kT}\right) \tag{37}$$

where n_i is the intrinsic carrier concentration, and τ is the minority-carrier lifetime. If the forward current is a result of recombination due to diffusing minority carriers (holes in n-type in this case), the characteristic should vary as

$$I = \frac{2qn_i^2 L_o A}{N_D \tau} \exp\left(\frac{qv}{kT}\right) \tag{38}$$

where L_o is the diffusion length of holes in n-type material. The two parameters in this thermal forward conduction are the minority-carrier lifetime τ and the diffusion length L_o.

A lifetime τ can be found from the $\exp(qv/2kT)$ portion of the diode current; and this lifetime, coupled with the $\exp(qv/kT)$ portion of the current, can lead to a diffusion length L_o. The temperature variation in n_i will cause the saturation current I_o to vary as

$$I_o \propto \frac{T^{5/2}}{E} \exp\left(\frac{qV_g}{2kT}\right) \tag{39}$$

for recombination in the space-charge region and as

$$I_o \propto T^3 \exp\left(\frac{qV_g}{kT}\right) \tag{40}$$

for diffusion current. The temperature variation in I_o has led to the following values of band gap near 300 °K:

Diode	V_g (v)
D10	1.36 to 1.49
D150	1.22
D130	1.50

These values agree with expected values of 1.37 v at 300 °K. The lifetimes and diffusion length determined by analysis of the high-temperature forward current are given in Table 7. All of the lifetimes decreased as the temperature was lowered. In diode D10 this decrease was from $2.5 \cdot 10^{-9}$ sec at 300 °K to $2.5 \cdot 10^{-10}$ sec at 199 °K. The values of lifetime vary in the vicinity of 10^{-9} to 10^{-10} sec, which appear to be reasonable for GaAs. A diffusion length of 5μ for electrons in GaAs has been measured by Nelson and Dousmanis [Ref. 29]. The agreement found between this value of 5μ and the value of 5.3μ measured by analysis of the forward current may well be fortuitous.

TABLE 7. HIGH-TEMPERATURE DIODE LIFETIME AND DIFFUSION LENGTH

Diode	Lifetime (sec)	Diffusion Length (μ)
D10*	$2 \cdot 10^{-9}$	5.3
D340	$2 \cdot 10^{-10}$	---
D350	$5.6 \cdot 10^{-10}$	---
D150	$3.6 \cdot 10^{-10}$	---
D180	$2 \cdot 10^{-10}$	---
D130	10^{-10}	---

*Note: $\tau = 2.5 \cdot 10^{-9}$ sec at 300 °K
$\tau = 2.5 \cdot 10^{-10}$ sec at 199 °K

If the reverse current is due to thermal generation of carriers in the space-charge region, then the reverse current should increase with the widening of the space-charge region under reverse bias. The reverse current should saturate if it is due to thermal generation of carriers in the bulk [Ref. 1]. In only one of the diodes reported here was thermal current observed in the reverse direction. This diode, HPA-1, displayed a current indicating generation in the space-charge region at currents less than 10^{-10} amp at 300 °K only. The higher reverse current of this sample fitted more closely the tunnelling model. All other samples tested showed tunnelling components in the reverse direction larger than the thermal currents.

F. OTHER MATERIALS

Experiments were performed on two other materials in an attempt to observe excess tunnelling currents. The results of these tests showed that it was possible to have reasonable excess tunnelling at low temperatures if two criteria were met. First, the carriers on both sides of the junction must remain mobile at low temperatures. This implies a degenerate material at both room temperature and 4.2 °K. The second

criterion is a narrow space-charge region to allow the tunnelling probability to remain appreciable. This limits the maximum width constant to about 1000 Å. The two experiments performed on other materials consisted of tests on silicon p^+-n^+ diodes and on the junctions in indium antimonide transistors.

The indium antimonide junctions were the base-emitter and base-collector junctions of experimental transistors from Texas Instruments of Dallas, Texas. These transistors had current gains, β, between 20 and 50 at 77 °K. Above 120 °K these junctions became degenerate and good rectification was not obtained. Below 50 °K the carriers on one side of the junction froze out and double injection was observed.

The silicon diodes were grown junctions obtained from hp Associates. They consisted of 0.004 ohm-cm n-type material separated from 0.002 ohm-cm p-type material by an n-layer of 10 ohm-cm. All resistivities are given at room temperature. The measured width constant was between 500 and 1000 Å at 4.2 °K. The forward characteristic of one of these diodes is shown in Fig. 33 at 300 °K and 4.2 °K. The room-temperature characteristic is thermal current and the 4.2 °K current has the characteristics associated with excess tunnel current. The reverse current in this diode was dominated by band-to-band tunnelling at both 300 °K and 4.2 °K for voltages below the reverse breakdown voltage (about 7 v). Since the capacitance and area of these diodes could not be accurately determined, no data on the effective mass could be obtained.

The type of analysis applied to the reverse characteristics in Chapter 4, Sec. C has been applied to data taken by Lowen and Rediker [Ref. 30] on GaAs diodes. The reverse current and capacitance as a function of applied voltage have been given by these authors for voltages less than 10 v at $T = 300$ °K. Their starting material was doped at $N_D = 3.5 \cdot 10^{16}$ cm^{-3}.

If the current reported by these authors was tunnelling current, a plot of

$$\log\left[\frac{J}{V_a(V_a + V_g)C}\right] \quad \text{vs} \quad [C(V_a + V_g)]^{-1}$$

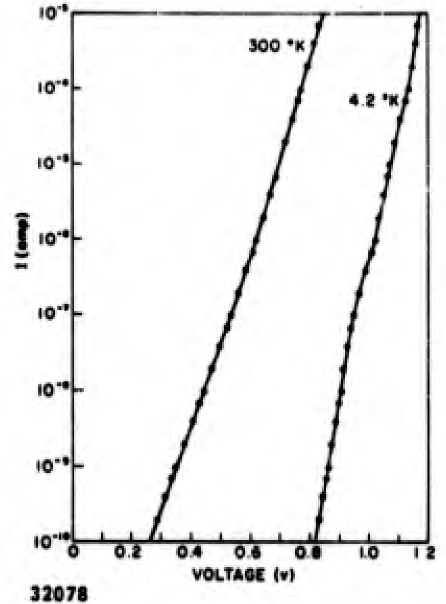

FIG. 35. FORWARD I-V CHARACTERISTIC OF SILICON DIODE HPA-69.

should yield a straight line. This plot is shown in Fig. 36 for voltages between 5 and 10 v. The two axes are given in arbitrary units. The data would yield an effective mass of 0.05 m_o if the diode area were $1.4 \cdot 10^{-5}$ cm^2, or if the diode diameter were about 0.002 in. The authors give their diode diameters as about 0.005 in. Thus the data of Lowen and Rediker are seen to agree reasonably well with the reverse tunnelling model described in this investigation.

G. SEPARATION OF CURRENTS INTO DIFFERENT COMPONENTS

The forward I-V characteristic in the temperature range from 4.2 to 300 °K can be described in terms of the three components of currents: diffusion current, recombination in the space-charge-region current, and tunnelling current. The diode characteristic is of the form

$$I = I_o(\text{dif}) \exp\left(\frac{qv}{1kT}\right) + I_o(\text{rec}) \exp\left(\frac{qv}{2kT}\right) + I_o(\text{tun}) \exp(\alpha v) \tag{41}$$

where $I_o(\text{dif})$ is the saturation current of the diffusion component, $I_o(\text{rec})$ is the saturation component of the recombination in the

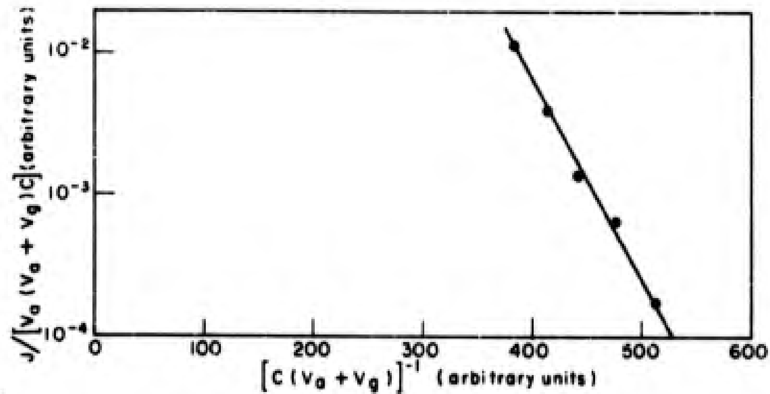

32079

FIG. 36. REVERSE DATA OF LOWEN AND REDIKER AS ANALYZED BY APPLYING REVERSE TUNNELLING MODEL AT T = 300 °K.

space-charge-region current, and $I_o(tun)$ is the saturation component of tunnelling current. The values of I_o and α measured on diode D10 are shown in Table 8. The measured decrease in lifetime has been included in the calculation of $I_o(rec)$ and $I_o(dif)$. The recombination probability of 10^{-5} and the measured temperature variation in V_{bi} have been included in the calculation of $I_o(tun)$. The components of current have been plotted in Fig. 37. Figure 37a shows the current due to recombination in the space-charge region, Fig. 37b shows the diffusion current, and Fig. 37c shows the tunnelling current. Notice that the thermal currents at temperatures below 100 °K become very small compared to the

TABLE 8. SATURATION CURRENTS OF DIODE D10 AT TEMPERATURES BETWEEN 4.2 AND 300 °K

Temperature (°K)	$I_o(dif)$ (amp)	$I_o(rec)$ (amp)	$I_o(tun)$* (amp)
300	10^{-20}	10^{-13}	10^{-21}
200	10^{-30}	10^{-18}	10^{-22}
100	10^{-67}	10^{-40}	$3 \cdot 10^{-23}$
4.2	---	---	10^{-23}

*$\alpha = 29\ v^{-1}$ in low-temperature tunnelling currents.

tunnelling current for biases less than 1.3 v. The measured forward I-V characteristic at temperatures between 4.2 and 300 °K and the fit of this current to the sum of the three components are shown in Fig. 38 for diode D10. The dominance of tunnelling in the low-level forward current at low temperatures is clearly presented in this figure.

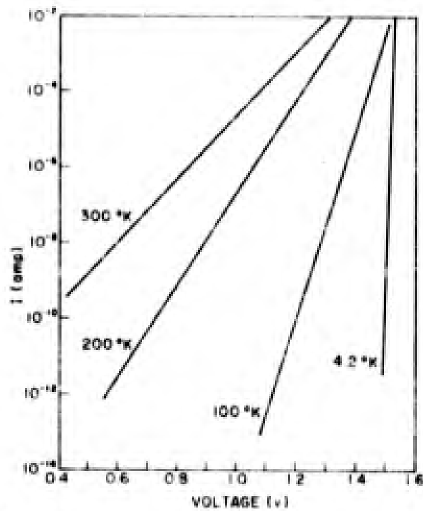

32080

a. Due to recombination in the space-charge region

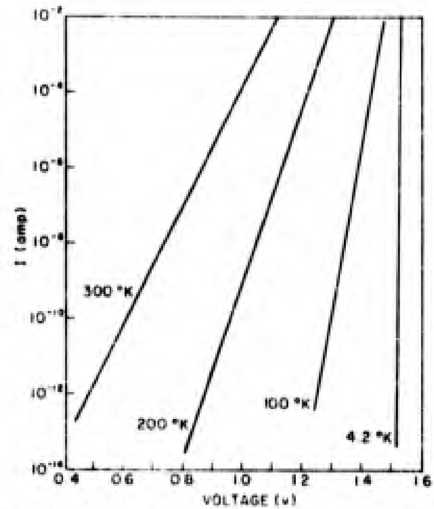

32081

b. Diffusion current

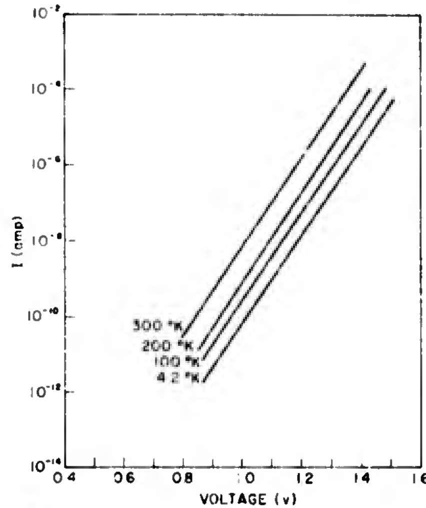

32082

c. Tunnelling current

FIG. 37. FORWARD CURRENT FOR TEMPERATURES BETWEEN 300 °K AND 4.2 °K.

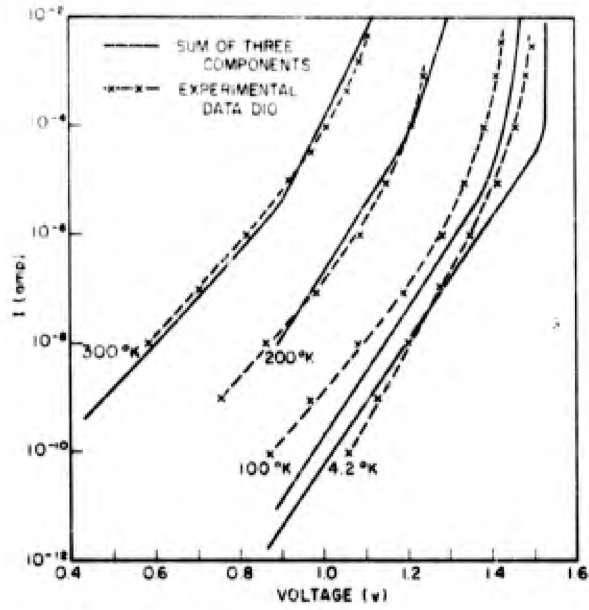

32083

FIG. 38. EXPERIMENTAL DATA AS THE SUM OF THREE COMPONENTS OF CURRENT.

V. RESULTS AND DISCUSSION

The discussion of the results of this investigation centers upon the explanation of the high-temperature diode properties in terms of existing thermal models, and the low-temperature properties in terms of a tunnelling model.

The low-temperature diode forward conduction has been discussed in terms of a band-to-trap-to-band tunnelling model. With the exception of one heavy mass and one light mass, the effective mass of the tunnelling particle has been found to vary between 0.017 m_o and 0.079 m_o at 4.2 °K. These values scatter around the reduced hole-electron effective mass of 0.063 m_o and appear to be reasonable values to observe. The lighter effective masses in general are associated with the more lightly doped materials. The majority of the effective masses are smaller than the reduced hole-electron mass. The low effective masses could be attributed to tunnelling near localized imperfections since this could lead to effective diode areas smaller than those measured photographically. Smaller diode areas would in essence steepen the curves presented in Fig. 23, which would lead to higher effective masses.

The recombination probability was introduced to account for the fact that the measured currents were much smaller than predicted on the basis of a band-to-band tunnelling picture. The physical significance associated with this quantity is that it represents the condition of the end state of the tunnelling process. This is probably an oversimplification. It is probably a combination of initial state effects and end state effects. If the high conductivity of the n-type GaAs at low temperatures is due to impurity band conduction, then the integration that leads to the average electron velocity as given in Eq. (10) is not correct. A lower value of average particle velocity will result if the low-temperature conduction is due to impurity banding. Thus the interpretation of the recombination probability as a function of temperature was described in the loosest terms.

The high-temperature forward conduction current was found to be thermal current in the lightly doped materials, and tunnel current in the heavily doped materials. The lifetime of minority carriers (probably holes injected into n-type) was observed to be about 10^{-10} to 10^{-9} sec, with a

corresponding diffusion length of 5μ at high temperatures. The separation of currents as shown in Figs. 37 and 38 demonstrates the three components of current that make up the diode characteristic.

The reverse characteristics fitted a tunnelling model from 4.2 to 300 °K. Except for two cases of very low effective mass, the effective masses varied from 0.018 to 0.099 m_o at 4.2 °K. As in the case of the forward characteristics, the low effective mass could be associated with tunnelling in the vicinity of local imperfections. The functional form of the observed current fits very well the tunnelling model. The magnitudes of the observed reverse currents fit reasonably well the theoretical predictions as displayed in Fig. 32.

The demonstration of the temperature-independent slope of the log I-V characteristics in silicon-grown junctions indicates that the forward excess current conduction mechanism can be observed in materials at low temperatures in which two criteria are met: the carriers must remain mobile at low temperatures and the space-charge region must be sufficiently narrow to allow an appreciable tunnelling probability. The space-charge region should be less than about 1000 Å in order to retain a reasonable tunnelling probability.

The results of the work performed on the low-temperature forward I-V characteristics of GaAs diodes can be summarized by returning to the original statement of the problem. There the I-V characteristic was seen to have a current that varied as $\exp(qv/2kT)$ at high temperatures and $\exp(\alpha v)$ at low temperatures. An "effective low temperature," T_{eff}, to be applied to the low-temperature characteristics could be defined by the equation

$$\frac{qv}{2kT_{eff}} = \alpha v \quad . \tag{42}$$

or

$$T_{eff} = \frac{q}{2k\alpha} \tag{43}$$

For a step junction, T_{eff} depends on the square root of the doping density. Using the value of α found previously for step junctions and given by Eq. (22b), yields the effective low temperature of the junction

$$T_{eff} = \frac{2q\hbar N_D^{1/2}}{\pi k m_T^{1/2} \epsilon^{1/2}} \tag{44}$$

This effective low temperature is plotted as a function of the doping density in Fig. 39 using $m_T = 0.063 m_o$ and the maximum field approximation.

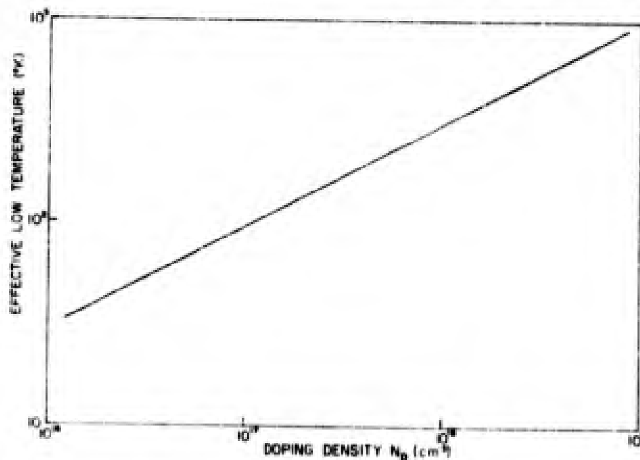

FIG. 39. EFFECTIVE LOW TEMPERATURE FOR STEP JUNCTIONS AS A FUNCTION OF DOPING DENSITY.

The effective low temperature has the following significance. For junction temperatures such that $T > T_{eff}$, the junction behaves like a normal diode with a characteristic that varies as $\exp(qv/2kT)$. For temperatures such that $T < T_{eff}$, the junction behaves like a diode but with $T = T_{eff}$, and displays a characteristic of the form $\exp(qv/2kT_{eff})$. The factor of 2 in $\exp(qv/2kT)$ may disappear in narrow band-gap materials such as germanium.

A GaAs step junction produced by diffusion of zinc into n-type material of doping density $N_D = 9.4 \cdot 10^{17}$ cm^{-3} could produce interesting results. If a characteristic of the form exp (qv/2kT) was observed at room temperature, it would not be possible to determine whether this current was thermal current due to recombination in the space-charge region or tunnelling current with an effective low temperature of 300 °K. Capacitance and area measurements--or measurements of diode current at different temperatures--would have to be made to distinguish between the two types of current. One sample, D320, was made from a parent doped at $1.8 \cdot 10^{18}$ cm^{-3}. This diode had a room-temperature characteristic of the form $I = I_o \exp(qv/2.2kT)$. The temperature dependence of this current indicated that this diode was conducting at room temperature via tunnelling currents with $T_{eff} = 330$ °K.

An application of this characteristic might be in producing a diode which had an exponential voltage dependence, the exponent being independent of temperature over a wide range of temperatures. For example, diode D160 had an effective low temperature of $T_{eff} = 450$ °K at temperatures below 300 °K. Thus this diode could be used at temperatures below 450 °K and the diode would retain its $\exp[qv/2k(T = 450\ °K)]$ characteristic. The doping density corresponding to 300 °K is found from Fig. 39 as $N_D = 9.4 \cdot 10^{17}$ cm^{-3}.

VI. CONCLUSIONS

An explanation has been sought for the conduction mechanism taking place in forward-biased GaAs diodes at low temperatures. The temperature-independent exponential behavior has been explained in terms of a tunnelling model. The forward I-V characteristic has been characterized by two parameters, the effective mass and the recombination probability. The effective mass is used to fit the exponent of the I-V characteristic and the recombination probability is used to scale the magnitude. The effective masses found from the forward I-V characteristic tend to scatter around the reduced hole-electron mass of 0.063 m_o. The recombination probability generally falls between 10^{-3} and 10^{-7} and seems to be an indication of the end state effects involved in the tunnelling process.

The high-temperature forward I-V data fit well the existing recombination models with minority-carrier lifetimes between 10^{-9} and 10^{-10} sec, and a minority-carrier diffusion length of 5μ. These two values appear reasonable in the light of current knowledge about GaAs.

The forward current-voltage characteristics have been analyzed in terms of three components. The first two are the normal thermal components which have an exp (qv/nkT) behavior, where $1 < n < 2$. The third component of current is the tunnelling current which will dominate the I-V characteristic at various temperatures. The temperature at which the tunnelling component becomes important is strongly determined by the doping density of the parent, since this doping density determines the width of the space-charge region and hence the tunnelling probability. A quantity, the effective low temperature, has been introduced to characterize the low-temperature tunnelling current.

The reverse currents have been compared with a band-to-band tunnelling model at all temperatures between 300 °K and 4.2 °K. The functional form of the observed reverse current fits the tunnelling model over as much as five or six decades of current. The effective tunnelling masses found from the reverse characteristics tend to scatter around the reduced hole-electron mass. The magnitudes of the observed reverse currents compare well with the tunnelling current calculated using the maximum field - effective mass approximation.

There may be promise in extending this work in the future to study states in the forbidden gap. A silicon on GaAs diode having the exponential characteristic such as is found in the D160 in essence sweeps out the entire band gap as forward voltage is applied. Introduction of high density of traps at localized energies should be observable as increases in the current when the applied voltage reaches the trap energy level. A material such as GaAs might be suitable for this study since the electron mass is much lower than the hole mass and recombination through tunnelling holes might be reduced.

REFERENCES

1. W. Shockley, Bell Sys. Tech. J., 35, 1956, p. 1.
2. C. T. Sah, R. N. Noyce, and W. Shockley, Proc. IRE, 45, 1957, p. 1228.
3. M. A. Lampert, Phys. Rev., 125, 1962, p. 126.
4. G. E. Smith and D. Kahng, Solid State Elect., 5, 1962, p. 177.
5. L. Esaki, Phys. Rev., 109, 1958, p. 603; L. Esaki and Y. Miyahara, Solid State Elect., 1, 1960, p. 13.
6. A. G. Chynoweth, W. L. Feldmann, and R. A. Logan, Phys. Rev., 121, 1961, p. 684.
7. A. G. Chynoweth, et al, Phys. Rev., 118, 1960, p. 425.
8. B. G. Cohen, W. B. Snow, and A. R. Tretola, Rev. Sci. Instr., 34, 1963, p. 1091.
9. D. F. Nelson, et al, Appl. Phys. Lett., 2, 1963, p. 182.
10. R. J. Archer, et al, Phys. Rev. Lett., 10, 1963, p. 483.
11. J. L. Powell and B. Craseman, Quantum Mechanics, Addision-Wesley Publishing Co., Reading, Mass., 1961.
12. L. V. Keldysh, Soviet Phys.-JETP 6(33), 1958, p. 763; L. V. Keldysh, Soviet Phys.-JETP 7(34), 1958, p. 665; and E. O. Kane, J. Appl. Phys., 32, 1961, p. 83.
13. H. Ehrenreich, Phys. Rev., 120, 1960, p. 1951.
14. J. E. Mayer and M. G. Mayer, Statistical Mechanics, John Wiley & Sons, New York, 1940.
15. E. Spenke, Electronic Semiconductors, McGraw-Hill Book Co., Inc., New York, 1958.
16. J. Blanc, R. H. Bube, and H. E. Macdonald, J. Appl. Phys., 32, 1961, p. 1666; R. W. Hamaker and H. F. Quinn, J. Appl. Phys., 33, 1962, p. 2396.
17. J. C. Penley, Phys. Rev., 128, 1962, p. 596.
18. N. Holonyak, et al, Phys. Rev. Lett., 4, 1959, p. 456.
19. R. S. Claassen, J. Appl. Phys., 32, 1961, p. 2372.
20. J. L. Moll, Physics of Semiconductors, McGraw-Hill Book Co., Inc., New York, 1964.
21. J. G. Linvill and J. F. Gibbons, Transistors and Active Circuits, McGraw-Hill Book Co., Inc., New York, 1961.
22. H. C. Casey, Jr., "Fabrication of Gallium Arsenide Subnanosecond Switching Diode," Rept. SEL-62-066 (TR No. 1802-1), Stanford Electronics Laboratories, Stanford, Calif., May 1962.

23. Quarterly Research Review No. 6, Rept. SEL-63-113, Stanford Electronics Laboratories, Stanford, Calif., 1 Jul - 30 Sep 1963, pp. II-32 - II-34.

24. J. E. Iverson, A. R. Bray, and J. J. Kleimack, IRE Trans., ED-9, 1962, p. 474.

25. R. N. Hall and J. H. Racette, J. Appl. Phys., 35, 1964, p. 379.

26. D. N. Nasledov, J. Appl. Phys., 32, 1961, p. 2140.

27. J. J. Tiemann and H. Fritzsche, Phys. Rev., 132, 1963, p. 2506.

28. C. W. Bates, Jr., Phys. Rev., 121, 1961, p. 1070.

29. H. Nelson and G. C. Dousmanis, Appl. Phys. Lett., 4, 1964, p. 192.

30. J. Lowen and R. H. Rediker, J. Elect. Chem. Soc., 107, 1960, p. 26.

SOLID STATE DISTRIBUTION LIST

August 1964

GOVERNMENT

USAEL
Ft. Monmouth, New Jersey
1 Attn: AMSEL-RD SL-PF
Dr. Harold Jacobs

Commanding General
USAEL, Bldg. 42
Ft. Monmouth, New Jersey
5 Attn: AMSEL-RD SL-SC

Commanding Officer
USAEL
Ft. Monmouth, New Jersey
1 Attn: AMSEL-RD TNR
1 Attn: Data Equipment Branch

Commanding Officer
USAEL
Ft. Monmouth, New Jersey
1 Attn: SIGFM EL PEP
R. A. Gerhold
1 Attn: AMSEL-RD/SL-PRT, M. Zinn
1 Attn: AMSEL-RD SL-PRT

Engineering Procedures Br.
U.S. Army Signal Materiel
Support Agency
Ft. Monmouth, N.J.
1 Attn: Millard Rosenfeld

Commanding Officer
Frankford Arsenal
Library Branch 0270, Bldg. 40
Bridge and Tacony Streets
1 Philadelphia 37, Pa.

Ballistics Research Lab.
Aberdeen Proving Ground, Md.
2 Attn: V. W. Richard, BML
1 Attn: Ballistics Res. Lab.
K.A. Pullen
1 Attn: Chief, Computer Res. Br.

Chief of Naval Research
Dept. of the Navy
Washington 25, D.C.
2 Attn: Code 427
2 Attn: Code 437, Inf. Syst. Br.

Commanding Officer
Office of Naval Research
Branch Office
1000 Geary St.
1 San Francisco 9, Calif.

Chief Scientist
Office of Naval Research
Branch Office
1030 E. Green St.
1 Pasadena, Calif.

San Francisco Ordnance Dist.
Basic Research and Special
Projects Br.
P. O. Box 1829, 1515 Clay St.
Oakland 12, Calif.
1 Attn: Mr. M. B. Sundstrom, Chief

ONR
Branch Office Chicago
230 N. Michigan Ave.
1 Chicago 1, Ill.

Commanding Officer
ONR Branch Office
495 Summer Street
1 Boston 10, Mass.

U.S. Army Electr. Labs.
Mt. View Office
P. O. Box 205
1 Mt. View, Calif.

Commanding Officer
ONR Branch Office
207 West 24th St.
New York 11, N.Y.
1 Attn: Dr. I. Rowe

U.S. Naval Applied Science Lab.
Tech. Library
Bldg. 291, Code 9832
Naval Base
1 Brooklyn, N.Y. 11251

Officer-in-Charge
Office of Naval Research
Navy No. 100, Box 39
Fleet Post Office
16 New York, N.Y.

U.S. Naval Research Lab.
2 Washington 25, D.C.
6 Attn: Code 2000
1 Attn: Code 5240
1 Attn: Code 5430
1 Attn: Code 5200
1 Attn: Code 5300
1 Attn: Code 5400
1 Attn: Code 5266, G. Abraham
1 Attn: Code 5260
1 Attn: Code 6430

Chief, Bureau of Ships
Navy Dept.
2 Washington 25, D.C.
1 Attn: Code 732, Mr. A. E. Smith
1 Attn: Code 335
1 Attn: Code 684A, R. Jones
1 Attn: Code 686
1 Attn: Code 687E
1 Attn: Code 687D
3 Attn: Code 670B
1 Attn: Code 681A1D
1 Attn: Code 691A1
1 Attn: Code 670 NTDS
1 Attn: Code 607A LCDR
E. B. Mashinke
1 Attn: Code 681A

Chief, Bureau of Naval Weapons
Navy Dept.
Washington 25, D.C.
1 Attn: RAAV 6

Chief, Bur. of Naval Weapons
Navy Dept.
Washington 25, D.C.
2 Attn: RREN-3
1 Attn: RAAV-44
1 Attn: ASW Detection and Control Div.
1 Attn: RMWC, Missile Weapons Control Div.
1 Attn: DIS-31
1 Attn: RAAV, Avionics Div.

Chief of Naval Operations
Navy Dept.-Pentagon 4C717
Washington 25, D.C.
1 Attn: Op 94T
1 Attn: Op 07T 12

Commanding Officer & Dir.
U.S. Navy Electronics Lab.
San Diego 52, Calif.
1 Attn: Tech. Library

U.S. Naval Post Grad. Sch.
Monterey, Calif.
1 Attn: Tech. Reports Library

Weapons Systems Test Div.
Naval Air Test Center
Patuxent River, Md.
1 Attn: Library

U.S. Naval Weapons Lab.
Dahlgren, Va.
1 Attn: Technical Library
1 Attn: G. H. Gleissner,
Computation Div.

U.S. Naval ORD Test Station
Pasadena Annex
3202 E. Foothill Blvd.
1 Attn: Tech. Library (Code P8C962)

U.S. Army R and D Lab.
Ft. Belvoir, Va.
1 Attn: Tech. Doc. Ctr.

U.S. Naval Weapons Lab.
Dahlgren, Va.
1 Attn: Computation and Analysis
Lab.

U.S. Naval Ordnance Lab.
Corona, Calif.
1 Attn: Robert Conger, 423
1 Attn: H. H. Wieder 423

Commanding Officer (ADL)
U.S. Naval Air Devel. Center
1 Johnsville, Pa. 18974

U.S. Naval Avionics Facility
Indianapolis 18, Ind.
1 Attn: Station Library

Naval Ordnance Lab.
White Oaks
Silver Spring 19, Md.
1 Attn: Tech. Library

Commanding Officer
U.S. Army Materiel Command
Washington 25, D.C.
1 Attn: AMCRD-DE-E
1 Attn: AMCRD-RS-PE-E

Commanding Officer
U.S. Army Research Office
(Durham)
Box CM, Duke Station
Durham, N.C.
3 Attn: CRD-AAIP

Dept. of the Army
Office, Chief, Research and Dev't.
Room 3D442, Pentagon
Washington 25, D.C.
1 Attn: Research Support Div.

Commanding General
USAEL
1 Attn: Technical Documents Ctr.
Evans Signal Lab. Area,
Bldg. 27
Ft. Monmouth, N.J.

Commander
Army Ballistic Missile Agency
1 Attn: ORDAB-DGC
Redstone Arsenal, Ala.

Advisory Group on Reliability of
Electronic Equipment
Office, Ass't Sect. of Defense
The Pentagon
1 Washington 25, D.C.

Commanding General
U.S. Army Electronics Comm.
Attn: AMSEL-AD
1 Ft. Monmouth, N.J.

Office, Chief of Res. and Dev't
Dept. of the Army
3045 Columbia Pike
Arlington 4, Va.
1 Attn: L.H. Geiger, Res. Planning Div.

Office of the Chief of Engineers
Chief, Library Branch
Dept. of the Army
1 Washington 25, D.C.

Chief of Staff
U.S. Air Force
Washington 25, D.C.
2 Attn: AFDRT-ER

U.S. Army Signal Liaison Office
ASD
Wright-Patterson AFB, Ohio
1 Attn: ASDL - 9

Commander
Aeronautical Systems Div.
Wright-Patterson AFB, Ohio
1 Attn: ASRNE-2, Mr. D. R. Moore
1 Attn: ASRNRS-2
2 Attn: ASRNEM
1 Attn: ASRNE-32
1 Attn: WWKSC-M, Mergulis

Systems Engr. Group (RTD)
Wright-Patterson AFB, Ohio 45433
1 Attn: SEPIR

Commandant
AF Institute of Technology
Wright-Patterson AFB, Ohio
1 Attn: AFIT-Library

DFEE, Lib. Officer
USAF Academy
1 USAF Academy, Colorado

Executive Director
Air Force Office of Scientific Research
Washington 25, D.C.
1 Attn: Code SRPP
1 Attn: Code SREE

Office of Scientific Res.
Dept. of the Air Force
Washington 25, D.C.
1 Attn: SRGL

AFWL (WLL)
2 Kirtland AFB, N.M.

Director, Air Univ. Library
Maxwell AFB, Alabama
1 Attn: CR 4582

AFSC Liaison Office
Los Angeles Area
1 Attn: Lt. Col. A.A. Konkel
6331 Hollywood Blvd.
Hollywood 28, Calif.

Hq. USAF (AFRDR-NO-3)
The Pentagon
1 Attn: Harry Mulkey
Rm 4D 335
Washington 25, D.C.

Air Force Systems Command
Scientific and Tech. Liaison Office
111 E. 16th St.
1 New York 23, N.Y.

School of Aerospace Medicine
USAF Aerospace Medical Div.
AFSC, Brooks AFB, Texas
1 Attn: SMAP

Commanding General
Rome Air Dev't. Center
Griffiss AFB, Rome, N.Y.
1 Attn: RCWID, Maj. B.J. Long
1 Attn: RCIMA, J. Dove

Commanding General
Air Force Cambridge Res. Labs.
Air Res. and Dev't. Command
L. G. Hanscom Field
Bedford, Mass.
1 Attn: CRTOTT-2, Electronics
1 Attn: Elec. Res. Lab. (CRR)
1 Attn: Chief, CRB

Data Sciences Lab, CRB
AFCRL
L. G. Hanscom Field
Bedford, Mass. 01731
1 Attn: Dr. H. H. Zschirnt
Senior Scientist

Headquarters, AFSC
Attn: SCTAE
Andrews AFB,
1 Washington 25, D.C.

Ass't Sect. of Defense (Research and Dev't)
Dept. of Defense
Washington 25, D.C.
1 Attn: Technical Library

Office of Director of Defense
Research and Engineering
Dept. of Defense
1 Washington 25, D.C.

Nat'l Aeronautics and Space Admin.
Goddard Space Flight Center
Greenbelt, Md.
1 Attn: Chief, Data Systems Div.

Nat'l Aeronautics and Space Admin.
George C. Marshall Space Flight Center
Huntsville, Alabama
1 Attn: M-G and C-R

Ass't of Sect. of Defense for Res. and Engineering
Information Officer, Library Br.
Pentagon Bldg.
2 Washington 25, D.C.

Dept. of Defense
Defense Communications Agency
Washington 25, D.C.
1 Attn: 121A, Tech. Lib.

Institute for Defense Analyses
1666 Connecticut
Washington 9, D.C.
1 Attn: W. E. Bradley

David Taylor Model Basin
Washington 7, D.C.
1 Attn: Tech. Lib., Code 142

U.S. Coast Guard
1300 E. Street, N.W.
Washington 25, D.C.
1 Attn: EEE

Advisory Group on Electron Devices
346 Broadway, 8th Floor East
New York 13, N.Y.
2 Attn: Harry Sullivan

DDC (TISIA)
Cameron Station
20 Alexandria, Va.

Census Bureau
Washington 25, D.C.
1 Attn: Office of Ass't. Dir. for Statistical Services
J. L. McPherson

Program Director
Engineering Section
Nat'l Science Foundation
1 Washington 25, D.C.

Commanding Officer
Diamond Ordnance Fuze Labs.
Washington 25, D.C.
2 Attn: ORDTL 930, Dr. R.T. Young
1 Attn: Library
1 Attn: ORDTL-450-638, Mr. R. H. Comyn

Nat'l Bureau of Standards
Washington 25, D.C.
1 Attn: R. D. Elbourn
1 Attn: Mr. S.N. Alexander
1 Attn: Librarian

U.S. Dept. of Commerce
Nat'l Bureau of Standards
Boulder Labs.
Central Radio Propagation Lab.
1 Boulder, Colorado

U.S. Dept. of Commerce
Nat'l Bureau of Standards
Boulder Labs.
Boulder, Colorado
1 Attn: Miss J. Lincoln, Chief
Radio Warning Services Section

Director, Nat'l Security Agency
1 Ft. George G. Meade, Md.
1 Attn: R31
1 Attn: R42
1 Attn: Howard Campaigne
1 Attn: C3/TDL, Rm. 2C087, Tech. Doc.

Chief, U.S. Army Security Agency
Arlington Hall Station
2 Arlington 12, Va.

Central Intelligence Agency
2430 E. St., NW
Washington, D.C.
1 Attn: A. Borel

UNIVERSITIES

School of Engineering
Sciences
Arizona State University
1 Tempe, Arizona

University of Arizona
Elec. Engr. Dept.
Tucson 25, Arizona
1 Attn: Robert L. Walker
1 Attn: Dr. Douglas J. Hamilton
1 Attn: F. A. Lindholm

Jet Propulsion Lab.
Calif. Inst. of Technology
4800 Oak Grove St.
Pasadena 3, Calif.
1 Attn: Library

Univ. of Calif.
Elec. Engineering Dept.
Berkeley 4, Calif.
1 Attn: Prof. R.M. Saunders, Chm.

Univ. of Calif.
Radiation Lab.
Information Div., Bldg. 30,
Room 101
Berkeley, Calif.
1 Attn: Dr. R.K. Wakerling

Univ. of Calif.
Lawrence Radiation Lab.
P.O. Box 808
Livermore, Calif.
1 Attn: Tech. Info. Div.

Univ. of Calif. at Los Angeles
Los Angeles 24, Calif.
1 Attn: Dept of Engineering
Prof. Gerald Estrin
1 Attn: Electromagnetics Div.,
R.S. Elliott
1 Attn: C.R. Viswanathan,
SS Electr. Lab.

Univ. of Chicago
Institute for Computer Research
Chicago 37, Illinois
1 Attn: Nicholas C. Metropolis

Columbia University
New York 27, N.Y.
1 Attn: Dept. of Physics
Prof. L. Brillouin
1 Attn: Columbia Radiation Lab.

Cornell University
Cognitive Systems Res. Program
Hollister Hall
Ithaca, N.Y.
1 Attn: F. Rosenblatt

Univ. of Florida
Dept. of Elect. Engr.
Rm. 336, Engineering Bldg.
Gainesville, Florida
1 Attn: M.J. Wiggins

George Washington Univ.
Washington, D.C.
1 Attn: Prof. N. Grisamore

Drexel Inst. of Tech.
Dept. of Elect. Engr.
Philadelphia 4, Pa.
1 Attn: F.B. Haynes

Georgia Inst. of Tech.
Atlanta, Ga.
1 Attn: Mrs. J.H. Crosland
Librarian

Harvard University
Technical Reports Collection
Rm. 303A, Pierce Hall
Cambridge 38, Mass.
2 Attn: Mrs. Elizabeth Farkas,
Librarian

Harvard University
Pierce Hall 217
Cambridge 38, Mass.
1 Attn: Div. of Engineering and
Applied Physics
Dean Harvey Brooks

Univ. of Ill.
Elect. Engineering Res. Lab.
Urbana, Ill.
1 Paul D. Coleman, Rm. 218
1 Attn: William Perkins

University of Ill.
Digital Computer Lab.
Urbana, Ill.
1 Attn: Dr. J. E. Robertson

Univ. of Ill.
Coordinated Science Lab.
Urbana, Ill.
1 Attn: Prof. Daniel Alpert

Univ. of Ill.
Library Serials Dept.
1 Urbana, Ill.

Univ. of Ill.
Dept. of Physics
Urbana, Ill.
1 Attn: Dr. John Bardeen

Johns Hopkins Univ.
Applied Physics Lab.
8621 Georgia Ave.
Silver Spring, Md.
1 Attn: A.W. Nagy
1 Attn: N.H. Choksy
1 Attn: Document Library
1 Attn: Supervisor of Tech.
Reports

Carlyle Barton Labs.
Johns Hopkins Univ.
Charles and 34th Sts.
Baltimore 18, Md.
1 Attn: Librarian

Linfield Research Inst.
McMinnville Oregon
1 Attn: Guy . Hickok, Dir.

Marquette Univ.
Dept. of Elect. Engr.
1515 W. Wisconsin Ave.
Milwaukee 3, Wis.
1 Attn: Arthur C. Moeller

State Univ. of Iowa
Dept. of Electrical Engineering
Iowa City, Iowa
1 Attn: Prof. Donald L. Epley

M.I.T.
Cambridge 39, Mass.
1 Research Lab. of Electronics
(Document Rm. 26-327)
1 Lab. of Insulation Research
Miss Sils, Librarian, Rm 4-244

Lincoln Lab.
M.I.T.
P.O. Box 73
Lexington 73, Mass.
1 Attn: Dr. Walter I. Wells
1 Attn: Library
1 Attn: Navy Representative
1 Attn: Kenneth L. Jordan, Jr.

Dynamic Analysis and Control Lab.
M.I.T.
Rm. 3-457
Cambridge, Mass.
1 Attn: D. M. Baumann

Director, Cooley Electronics
Lab., N. Campus
Univ. of Mich.
1 Ann Arbor, Mich.

Univ. of Mich.
Dept. of Elect. Engr.
3503 E. Engineering Bldg.
Ann Arbor, Mich.
1 Attn. Prof. Joseph E. Rowe

Univ. of Mich.
180 Frieze Bldg.
Ann Arbor, Mich.
1 Attn: Dr. Gordon E. Peterson,
Dir. of Communication
Science Lab.

Univ. of Mich.
Inst. of Science and Tech.
Ann Arbor, Mich.
1 Attn: Tech. Documents Service

Univ. of Minn.
Dept. of Elect. Engr.
Inst. of Tech.
Minneapolis 14, Minn.
1 Attn: Prof. A. Van der Ziel

Univ. of Nevada
College of Engineering
Reno, Nev.
1 Attn: Dr. Robert A. Manhart,
Chm. Elect. Engr. Dept.

New York University
University Heights
New York 53, N.Y.
1 Attn: Dr. J. H. Mulligan, Jr
Chm. of EE Dept.

New York University
Solid State Lab.
4 Washington Pl.
New York 3, N.Y.
1 Attn: Dr. H. Kallmann

Northwestern Univ.
Aerial Measurements Lab.
2422 Oakton St.
Evanston, Ill.
1 Attn: Walter S. Toth

North Carolina State College
Dept. of E.E.
Raleigh, N.C.
1 Attn: Prof. Robert W. Lade

Univ. of Notre Dame
Elect. Engr. Dept.
South Bend, Indiana
1 Attn: Eugene Henry

Ohio State University
Dept. of Elect. Engr.
Columbus 10, Ohio
1 Attn: Prof. E.M. Boone

Oregon State Univ.
Dept. of Elect. Engr.
Corvallis, Oregon
1 Attn: H.J. Oorthuys

Univ. of Pennsylvania
Moore School of E.E.
200 S. 34th St.
Philadelphia 4, Pa.
1 Attn: Miss A.L. Campion

Polytechnic Institute
Elect. Engr. Dept.
333 Jay St.
1 Attn: Leonard Shaw

Polytechnic Inst. of Brooklyn
Graduate Center
Rt. 110
Farmingdale, N.Y.
1 Attn: Librarian

Princeton Univ.
Elect. Engr. Dept.
Princeton, N.J.
1 Attn: Prof. F.S. Acton

Research Inst. of Advanced Studies
7212 Bellona Ave.
Baltimore, Md.
1 Attn: Dr. R.E. Kalman

Purdue Univ.
Elect. Engr. Dept.
Lafayette, Ind.
1 Attn: Library

Rensselaer Polytechnic Institute
School of Engineering
Troy, N.Y.
1 Atten: Kenneth E. Mortenson

Univ. of Rochester
Gavett Hall
River Campus Station
Rochester 20, N.Y.
1 Attn: Dr. Gerald H. Cohen

VARSI Library
Univ. of Santa Clara
1 Santa Clara, Calif.

Stanford Research Inst.
Menlo Park, Calif.
1 Attn: External Reports G-037

Stanford Research Inst.
Computer Lab.
Menlo Park, Calif.
1 Attn: H.D. Crane

Syracuse University
Dept. of Elec. Engr.
Syracuse 10, N.Y.
1 Attn: Dr. Stanford Goldman

Univ. of Tennessee
Dept. of E.E.
Ferris Hall
1 Knoxville, Tenn.

Texas Technological College
Lubbock, Texas
1 Attn: Dir. Inst. of Science Engineering, Office of Dean of Engr.

Univ. of Utah
Electrical Engineering Dept.
Salt Lake City, Utah
1 Attn: Richard W. Grow

Univ. of Virginia
Charlottesville, Va.
1 Attn: J.C. Wyllie, Alderman Library

Wayne State University
Detroit, Mich.
1 Attn: Prof. Harry Josselson
Dept. of Slavic Languages

University of Wisconsin
College of Engineering
Dept. of Electrical Engineering
Madison, Wisconsin
1 Attn: Mr. Thomas C. Gabriel

Engineering Library
Yale University
New Haven, Conn.
1 Sloane Physics Lab.
1 Dept. of Elect. Engr.
1 Dunham Lab.

INDUSTRY

Admiral Corporation
3800 Cortland St.
Chicago 47, Ill.
1 Attn: E.N. Roberson, Librarian

Airborne Instruments Lab.
Comac Road
Deer Park, L.I., New York
1 Attn: John Dyer, Vice Pres. and Tech. Director

AMELCO Semiconductor
P.O. Box 1030
Mt. View, Calif.
1 Attn: Frits J. Andeweg

Amperex Corporation
230 Duffy Ave.
Hicksville, L.I., New York
1 Attn: S. Barbasso, Proj. Eng.

Auerbach Corp.
1634 Arch St.
1 Philadelphia 3, Pa.

Autonetics
Div. of N. American Aviation
9150 E. Imperial Highway
Downey, Calif.
1 Attn: Tech. Library 3040-3

Bell Telephone Laboratories
Murray Hill Labs.
Murray Hill, N.J.
1 Attn: Dr. J.K. Galt
1 Attn: Dr. J. R. Pierce
1 Attn: Dr. S. Darlington
1 Attn: A. J. Grossman
1 Attn: Dr. M. Sparks
1 Attn: A. J. Morton
1 Attn: Dr. R. M. Ryder

Bendix Corp.
Research Labs. Division
Southfield (Detroit), Mich.
1 Attn: A.G. Peifer

Benson-Lehner Corp.
14761 California St.
Van Nuys, Calif.
1 Attn: George Ryan

Boeing Scientific Res. Labs.
P.O. Box 3981
Seattle 24, Wash.
1 Attn: Dr. E.J. Nalos
MS-1331
ORG. 1-8000

Bomac Laboratories, Inc.
Beverly, Mass.
1 Attn: Research Library

Columbia Radiation Lab.
538 W. 120th St.
1 New York, N.Y.

Convair--San Diego
A Div. of Gen. Dynamics Corp.
San Diego 12, Calif.
1 Attn: Engr. Library
Mail Zone 6-157

Cook Research Labs.
6401 W. Oakton St.
1 Morton Grove, Ill.

Cornell Aeronautical Lab.
4455 Genesee St.
Buffalo 21, N.Y.
1 Attn: D.K. Plummer
2 Attn: Library

Eitel-McCullough, Inc.
301 Industrial Way
San Carlos, Calif.
1 Attn: Research Librarian
1 Attn: W.R. Luebke

Electro-Optical Instruments, Inc.
125 N. Vinedo
Pasadena, Calif.
1 Attn: I. Weiman

Fairchild Semiconductor Corp.
4001 Junipero Serra Blvd.
Palo Alto, Calif.
1 Attn: Dr. V.H. Grinich

General Electric Co.
Defense Electronics Div., LMED
Cornell Univ.
Ithaca, N.Y.
1 Attn: Library
VIA: Commander
Aeronautical Systems Div.
Wright-Patterson AFB, Ohio
Attn: ASRNC-5
Donald E. Lewis

General Electric TWT Product Sect.
601 Calif. Ave.
Palo Alto, Calif.
1 Attn: C.C. Lob
1 Attn: Tech. Library

General Electric Co.
Research Lab.
P.O. Box 1088
Schenectady, N.Y.
1 Attn: Dr. Philip M. Lewis
1 Attn: V. L. Newhouse
Applied Physics

General Electric Co.
Electronics Park-Bldg. 3
Room 143-1
Syracuse, N.Y.
1 Attn: Documents Librarian
(Yolanda Burke)

General Electric Co.
Schenectady 5, N.Y.
1 Attn: Library, LME Dept.
Bldg. 28-501

General Telephone and Electronics Labs., Inc.
Bayside 60, N.Y.
1 Attn: Louis R. Bloom

Gilfillan Brothers
1815 Venice Blvd.
Los Angeles, Calif.
1 Attn: Engineering Library

Goddard Space Flight Center
Code 611
1 Greenbelt, Md.

The Hallicrafters Co.
5th and Kostner Ave.
1 Chicago 24, Ill.

Hewlett-Packard Co.
1501 Page Mill Rd.
1 Palo Alto, Calif.

Hoffman Electronics Corp.
Semiconductor Div.
1001 Arden Dr.
El Monte, Calif.
1 Attn: P.N. Russel, Tech. Dir.

Hughes Aircraft Co.
Florence at Teale St.
Culver City, Calif.
1 Attn: Tech. Library
Bldg. 6, Rm. C2048
1 Attn: Solid-State Group-M 107
1 Attn: Tech. Doc. Ctr., Bldg. 6,
Mail Station E-110

HRB Singer
Science Park
P.O. Box 60
State College, Pa.
1 Attn: Tech. Info. Center

Hughes Aircraft Co.
Bldg. 6, Mail Station E-150
Culver City, Calif.
1 Attn: A.S. Jerrems,
Aerospace Group

Hughes Aircraft Co.
Semiconductor Div.
P.O. Box 278
Newport Beach, Calif.
1 Attn: Library

Hughes Aircraft Co.
Bldg. 604, Mail Station C-213
Fullerton, Calif.
1 Attn: A. Eschner, Jr.
Ground Systems Group

Hughes Aircraft Co.
3011 Malibu Canyon Rd.
Malibu, Calif.
1 Attn: H.A. Iams, Res. Lab.

International Business Machines
Product Development Lab.
Poughkeepsie, N.Y.
1 Attn: E.M. Davis - (Dept. 362)

International Business Machines
Data Systems Div.
Box 390, Boardman Rd.
Poughkeepsie, N.Y.
1 Attn: J.C. Logue

IBM Research Library
Box 218
1 Yorktown Heights, N.Y.

International Business Machines
San Jose, California
1 Attn: Majorie Griffin

ITT Federal Labs.
500 Washington Ave.
Nutley, N.J.
1 Attn: Librarian, Ellis Mount

Lab. for Electronics, Inc.
1079 Commonwealth Ave.
Boston 15, Mass.
1 Attn: Dr. H. Fuller
1 Attn: Library

LEL, Inc.
75 Akron St.
Copiague, L.I., N.Y.
1 Attn: Robert S. Mautner

Lenkurt Electric Co.
San Carlos, Calif.
1 Attn: M.L. Waller, Librarian

Librascope, Div. of General
Precision, Inc.
808 Western Ave.
Glendale 1, Calif.
1 Attn: Engineering Library

Lockheed Missile and Space Co.
Dept. 67-33, Bldg. 324
P.O. Box 504
Sunnyvale, Calif.
1 Attn: G.W. Price

Lockheed Missile and Space Co.
Dept. 65-70, Bldg. 524
P.O. Box 504
Sunnyvale, Calif.
1 Attn: Dr. W.M. Harris

Lockheed Missile Systems Co.
Sunnyvale, Calif.
1 Attn: Tech. Info. Ctr. 50-14

Lockheed Missile and Space Co.
Palo Alto, Calif.
1 Attn: M.E. Browne-Dept. 52-40
Bldg. 202

The Martin Co.
P.O. Box 5837
Orlando, Florida
1 Attn: Engr. Library M.P. 30

Marquardt Aircraft Corp.
16555 Saticoy St.
P.O. Box 2013, -South Annex
Van Nuys, Calif.
1 Attn: Dr. Basun Chenge
Research Scientist

Melpar, Incorporated
Applied Science Div.
3000 Arlington Blvd.
Falls Church, Va.
1 Attn: Librarian

Micro State Electronics Corp.
1 Attn: A. L. Kestenbaum
152 Floral Ave.
Murray Hill, N.J.

Microwave Assoc., Inc.
North West Industrial Park
Burlington, Mass.
1 Attn: Dr. Kenneth Mortenson
1 Attn: Librarian

Microwave Electronics Corp.
3165 Porter Drive
Palo Alto, Calif.
1 Attn: Stanley F. Kaisel
1 Attn: M.C. Long

Minneapolis-Honywell Regulator
Company
Semiconductor Library
1177 Blue Heron Blvd.
1 Riviera Beach, Florida

The Mitre Corporation
Bedford, Mass.
1 Attn: Library

Monsanto Chemical Co.
800 N. Lindbergh Blvd.
St. Louis 66, Mo.
1 Attn: Edward Orban, Mgr.
Inorganic Development

Motorola, Semiconductor Prod. Div.
5005 E. McDowell Rd.
Phoenix, Ariz.
1 Attn: Dr. A. Lesk
2 Attn: Dr. R. M. Warner, Jr.
2 Attn: Library

Nat'l Biomedical Inst.
8600 16th St.
Silver Spring, Md.
1 Attn: Dr. R.S. Ledley

Nortronics
Palos Verdes Research Park
6101 Crest Rd.
Palos Verdes Estates, Calif.
1 Attn: Technical Info. Agency

Oak Ridge National Lab.
(Operated By)
Union Carbide Corp.
P.O. Box X
Oak Ridge, Tenn. 37831
1 Attn: Librarian

Pacific Semiconductors, Inc.
14520 S. Aviation Blvd.
Lawndale, Calif.
1 Attn: H.Q. North

Philco Corp.
Tech. Rep. Div.
P.O. Box 4730
Philadelphia 34, Pa.
1 Attn: F.R. Sherman, Mgr. Editor
Philco Tech. Rep. Div.

Philco Corp.
Lansdale Div.
Church Rd.
Lansdale, Pa.
1 Attn: John R. Cordor

Philco Scientific Lab.
Blue Bell, Pa.
1 Attn: Dr. J.R. Feldmeier,
Assoc. Dir. of Research
1 Attn: C.V. Bocciarelli
1 Attn: C.T. McCoy, Res. Advisor

Polarad Electronics Corp.
43-20 Thirty-Fourth St.
Long Island City 1, N.Y.
1 Attn: A.H. Sonnenschein
Ass't to the President

RCA, Surf. Comm. Div.
Front and Market Streets
Bldg. 17-C-6
Camden, N.J.
1 Attn: K.K. Miller, Mgr.
Minuteman Project Of.

RCA Labs.
Princeton, N.J.
1 Attn: Harwick Johnson
1 Attn: Dr. W.M. Webster

RCA
Bldg., 108-134
Moorestown, N.J.
1 Attn: H.J. Schrader

The Rand Corp.
1700 Main St.
Santa Monica, Calif.
1 Attn: Lib., Helen J. Waldron
1 Attn: Computer Science Dept.
Willis H. Ware

Raytheon Co.
Microwave and Power Tube Div.
Spencer Lab.
Burlington, Mass.
1 Attn: Librarian

Raytheon Manufacturing Co.
28 Seyon St.
Research Div.
Waltham, Mass.
1 Attn: Dr. Herman Statz
1 Attn: Librarian

Raytheon Corp.
Waltham, Mass.
1 Attn: Dr. H. Scharfman

Roger White Electron Devices, Inc.
Tall Oaks Rd. Laurel Ledges
1 Stamford, Conn.

Space Technology Labs, Inc.
One Space Park
Redondo Beach, Calif.
2 Attn: Tech. Library
Doc. Acquisitions

Space Tech. Labs., Inc.
Physical Research Lab.
P.O. Box 95002
Los Angeles 45, Calif.
1 Attn: D. Fladlein

Sperry Gyroscope Company
Div. of Sperry Rand Corp.
Great Neck, N.Y.
1 Attn: Leonard Swern (M.S.3T105)

Sperry Microwave Electronics Co.
Clearwater, Florida
1 Attn: John E. Pippin,
Res. Section Head

Sperry Electron Tube Div.
Sperry Rand Corp.
Gainesville, Florida
1 Attn: Librarian

Sylvania Electronic Defense Lab.
P.O. Box 205
1 Mountain View, Calif.
1 Attn: Optics Dept., Bldg. 4

Sylvania Electric Products, Inc.
500 Evelyn Ave.
1 Mt. View, Calif.

Sylvania Electronics System
Waltham Labs.
100 First Ave.
Waltham 54, Mass.
1 Attn: Librarian
1 Attn: Ernest E. Hollis

Technical Research Group
Route 110
1 Melville, N.Y. 11749

Texas Instruments Incorporated
Apparatus Div.
P.O. Box 6015
Dallas 22, Texas
1 Attn: M.E. Chun

Texas Instruments, Inc.
Semiconductor-Components Div.
P.O Box 5012
Dallas 22, Texas
2 Attn: Semiconductor Components
Library

Texas Instruments Inc.
Corporate Res. and Engr.
Technical Reports Service
P.O. Box 5474
1 Dallas 22, Texas

Tektronix, Inc.
P.O. Box 500
Beaverton, Oregon
4 Attn: Dr. Jean F. Delord
Dir. of Research

Varian Associates
611 Hansen Way
Palo Alto, Calif.
1 Attn: Tech. Library

Westinghouse Electric Corp.
Friendship Internat'l Airport
Box 746, Baltimore 3, Md.
1 Attn: G. Ross Kilgore, Mgr.
Applied Research Dept.
Baltimore Laboratory

Westinghouse Electric Corp.
Beulah Rd.
Pittsburgh 35, Pa.
1 Attn: Dr. G.C. Sziklai

Melbourne J. Hellstrom, Supv. Engr.
Westinghouse Electronics Corp.
Molecular Electronics Div.
Box 1836
1 Baltimore, Md. 21203

Westinghouse Electric Corp.
Research Laboratories
Beulah Rd., Churchill Boro
Pittsburgh 35, Pa.
1 Attn: J.G. Castle, Jr.-401-1B5
1 Attn: Solid State Dept.
1 Attn: R.E. Davis

Zenith Radio Corporation
6001 Dickens Ave.
Chicago 39, Ill.
1 Attn: Joseph Markin

FOREIGN RECIPIENTS

Northern Electric Co., Ltd.
Res. and Dev't Labs.
**P.O. Box 3511, Station "C"
1 Ottawa, CANADA

University of Ottawa
Dept. of Electrical Engr.
** Ottawa 2, CANADA
1 Attn: G. S. Glinsky
VIA: ASD, Foreign Release Off. (ASYF)
Wright-Patterson AFB, Ohio
Attn: J. Troyan

Dr. Sidney V. Soanes
Research Dept.
Ferranti-Packard Elect. Ltd.
**Industry St.
1 Toronto 15, Ontario, CANADA

Central Electronics Engr. Research Institute
* Pilani, Rajasthan, INDIA
1 Attn: Om P. Gandhi

Prof. Sanai Mito
Dept. of Applied Physics
Faculty of Engineering
Osaka City University
* 12 Nishi-Ogimachi, Kitaku
1 Osaka, JAPAN

Prof. Jose M. Borrego
Centro de Investigacion Y de Estudios
Avazados Del Instituto Politecnico Nacional
**Apartado Postal 26740
1 Mexico 14, D.F.

Prof. E.H. Rhoderick
**Manchester College of Science and Tech.
1 Manchester 1, ENGLAND

Mr. Heikki Ihantola
**Fiskars Electronics Lab.
1 Elimaenkatu 17, Helsinki, FINLAND

Prof. Takuo Sugano
Faculty of Engineering
University of Tokyo
Bunkyo-ku, Tokyo
1 JAPAN

Dr. Niels I. Meyer
Physics Dept.
The Technical University of Denmark
Lundtoftevej 100, Lyngby
1 Denmark

Prof. G. Bruun
Royal Technical University of Denmark
Ostervolgade 10, G.
1 Copenhagen K, Denmark

Dr. Georges Alon
E.N.S. Laboratoire des Hautes Energies
Orsay/Seine et Oise
1 B.P. No. 2, France

Dr. P. A. Tove
Fysiska Institutionen
Uppsala University
1 Uppsala, Sweden

Prof. W. E. Dahlke
Telefunken, GmbH
Soflinger Strasse 100
Postfach 627
Ulm/Donau
1 Germany

Dr. G. B. B. Chaplin
The Plessey Company (U.K.) Ltd.
Caswell, Towcester
1 Northants, England

Dr. D. H. Roberts
The Plessey Company (U.K.) Ltd.
Caswell, Towcester
1 Northants, England

Royal Radar Establishment
Physics Dept.
St. Andrews Rd.
Great Malvern, Worcs.
England
1 Attn: Dr. P. N. Butcher

National Physical Lab.
Teddington, Middlesex
England
1 Attn: Dr. A. M. Uttley

Swiss Federal Institute of Technology
Gloriastrasse 35
Zurich, Switzerland
1 Attn: Prof. M. J. O. Strutt

Prof. A. DeBock
University of Louvain
Institute of Physique
61 Rue de Namur
1 Louvain, Belgium

Dr. Maurice Bernard
Dept. PCM
CNET
Issy-Les-Moulineaux
Seine, France
1 Attn: Solid-State and Electron Devices

Prof. Karl Steinbuch
Institute fur Nachrichtenverarbeitung und Nachrichtenubertragung
Technische Hochschule Karlsruhe
1 Karlsruhe, Germany

* ONR '4 Reports ONLY
** AF 46 reports ONLY
VIA: ASD, Foreign Release Office (ASYF)
Wright-Patterson AFB
Ohio
Attn: J. Troyan

UNCLASSIFIED

Security Classification

DOCUMENT CONTROL DATA - R&D

(Security classification of title, body of abstract and indexing annotation must be entered when the overall report is classified)

1. ORIGINATING ACTIVITY (Corporate author)	2a. REPORT SECURITY CLASSIFICATION
Stanford Electronics Laboratories Stanford University, Stanford, Calif.	UNCLASSIFIED
	2b. GROUP

3. REPORT TITLE

LOW-TEMPERATURE PROPERTIES OF GALLIUM ARSENIDE DIODES

4. DESCRIPTIVE NOTES (Type of report and inclusive dates)

Technical Report

5. AUTHOR(S) (Last name, first name, initial)

David J. Dumin

6. REPORT DATE	7a. TOTAL NO. OF PAGES	7b. NO. OF REFS
September 1964	68 + ix	30

8a. CONTRACT OR GRANT NO.	9a. ORIGINATOR'S REPORT NUMBER(S)
ONR Contract Nonr 225(24)	Technical Report No. 5107-1 SEL-64-097
b. PROJECT NO.	
c.	9b. OTHER REPORT NO(S) (Any other numbers that may be assigned this report)
d.	

10. AVAILABILITY/LIMITATION NOTICES

foreign announcement and dissemination of this report by DDC is limited

11. SUPPLEMENTARY NOTES	12. SPONSORING MILITARY ACTIVITY
	U.S. Army Signal Corps, U.S. Air Force, and U.S. Navy (ONR)

13. ABSTRACT See page 2

DD FORM 1 JAN 64 1473

UNCLASSIFIED

Security Classification

14. KEY WORDS	LINK A		LINK B		LINK C	
	ROLE	WT	ROLE	WT	ROLE	WT
GALLIUM ARSENIDE						
SOLID-STATE DIODES						
SOLID-STATE DIODES, THERMAL EFFECTS						

INSTRUCTIONS

1. **ORIGINATING ACTIVITY:** Enter the name and address of the contractor, subcontractor, grantee, Department of Defense activity or other organization *(corporate author)* issuing the report.

2a. **REPORT SECURITY CLASSIFICATION:** Enter the overall security classification of the report. Indicate whether "Restricted Data" is included. Marking is to be in accordance with appropriate security regulations.

2b. **GROUP:** Automatic downgrading is specified in DoD Directive 5200.10 and Armed Forces Industrial Manual. Enter the group number. Also, when applicable, show that optional markings have been used for Group 3 and Group 4 as authorized.

3. **REPORT TITLE:** Enter the complete report title in all capital letters. Titles in all cases should be unclassified. If a meaningful title cannot be selected without classification, show title classification in all capitals in parenthesis immediately following the title.

4. **DESCRIPTIVE NOTES:** If appropriate, enter the type of report, e.g., interim, progress, summary, annual, or final. Give the inclusive dates when a specific reporting period is covered.

5. **AUTHOR(S):** Enter the name(s) of author(s) as shown on or in the report. Enter last name, first name, middle initial. If military, show rank and branch of service. The name of the principal author is an absolute minimum requirement.

6. **REPORT DATE:** Enter the date of the report as day, month, year; or month, year. If more than one date appears on the report, use date of publication.

7a. **TOTAL NUMBER OF PAGES:** The total page count should follow normal pagination procedures, i.e., enter the number of pages containing information.

7b. **NUMBER OF REFERENCES:** Enter the total number of references cited in the report.

8a. **CONTRACT OR GRANT NUMBER:** If appropriate, enter the applicable number of the contract or grant under which the report was written.

8b, 8c, & 8d. **PROJECT NUMBER:** Enter the appropriate military department identification, such as project number, subproject number, system numbers, task number, etc.

9a. **ORIGINATOR'S REPORT NUMBER(S):** Enter the official report number by which the document will be identified and controlled by the originating activity. This number must be unique to this report.

9b. **OTHER REPORT NUMBER(S):** If the report has been assigned any other report numbers *(either by the originator or by the sponsor)*, also enter this number(s).

10. **AVAILABILITY/LIMITATION NOTICES:** Enter any limitations on further dissemination of the report, other than those imposed by security classification, using standard statements such as:

(1) "Qualified requesters may obtain copies of this report from DDC."

(2) "Foreign announcement and dissemination of this report by DDC is not authorized."

(3) "U. S. Government agencies may obtain copies of this report directly from DDC. Other qualified DDC users shall request through ______________."

(4) "U. S. military agencies may obtain copies of this report directly from DDC. Other qualified users shall request through ______________."

(5) "All distribution of this report is controlled. Qualified DDC users shall request through ______________."

If the report has been furnished to the Office of Technical Services, Department of Commerce, for sale to the public, indicate this fact and enter the price, if known.

11. **SUPPLEMENTARY NOTES:** Use for additional explanatory notes.

12. **SPONSORING MILITARY ACTIVITY:** Enter the name of the departmental project office or laboratory sponsoring *(paying for)* the research and development. Include address.

13. **ABSTRACT:** Enter an abstract giving a brief and factual summary of the document indicative of the report, even though it may also appear elsewhere in the body of the technical report. If additional space is required, a continuation sheet shall be attached.

It is highly desirable that the abstract of classified reports be unclassified. Each paragraph of the abstract shall end with an indication of the military security classification of the information in the paragraph, represented as *(TS)*, *(S)*, *(C)*, or *(U)*.

There is no limitation on the length of the abstract. However, the suggested length is from 150 to 225 words.

14. **KEY WORDS:** Key words are technically meaningful terms or short phrases that characterize a report and may be used as index entries for cataloging the report. Key words must be selected so that no security classification is required. Identifiers, such as equipment model designation, trade name, military project code name, geographic location, may be used as key words but will be followed by an indication of technical context. The assignment of links, roles, and weights is optional.

ABSTRACT

The forward and reverse current-voltage characteristics of zinc-diffused gallium arsenide (GaAs) diodes have been investigated at temperatures between 300 and 4.2 °K. This study was initiated to explain the portions of the forward and reverse currents that are nonthermal in origin. The high-temperature current follows a law of the form $I = I_o \exp(qv/2kT)$. The low-temperature current follows a law of the form $I = I_1 \exp(\alpha v)$, where α is almost independent of temperature. The reverse current is higher at all temperatures and voltages than thermal-generation models predict and does not have the functional dependence associated with thermally generated currents.

Zinc-diffused GaAs diodes were produced and tested at temperatures between [illegible] and 4.2 °K. The doping densities of the parent materials ranged from $5 \cdot 10^{15}$ cm^{-3} to 10^{19} cm^{-3}. In addition to undoped n-type material, parent materials doped with selenium, sulfur, and tellurium were used. The p-type diffusions produced doping densities generally in the vicinity of 10^{20} cm^{-3}.

The high-temperature forward current has been explained in terms of existing thermal models using minority-carrier lifetimes of the order of 10^{-9} to 10^{-10} sec, and minority-carrier diffusion lengths of the order of 5μ. The low-temperature forward current has been explained in terms of a band-to-trap-to-band excess tunnelling model describable by two parameters: the effective tunnelling mass and the recombination probability. The effective tunnelling mass describes the exponent in the low-temperature current and the recombination probability describes the magnitude of the current. The effective masses observed in the forward direction scatter above and below the reduced hole-electron mass of 0.063 m_o. The temperature at which the tunnelling current dominates the forward characteristic rises as the doping density rises. The temperature at which the tunnelling current becomes appreciable has been described in terms of an "effective low temperature."

The reverse current has been explained in terms of a band-to-band tunnelling model at all temperatures below 300 °K. The effective tunnelling mass has been used as the parameter that describes the reverse current

and is observed generally to follow the effective masses found from the forward conduction. The experimentally measured reverse currents compare well with the theoretically predicted values.

The dominance of excess currents at low temperatures has been demonstrated in silicon in which two criteria are met: first, the carriers must remain mobile at low temperatures and, second, the space-charge region must be less than 1000 Å.

UNCLASSIFIED

UNCLASSIFIED